HHS Public Access

Author manuscript

J Comp Neurol. Author manuscript; available in PMC 2016 December 15.

Published in final edited form as:

J Comp Neurol. 2015 December 15; 523(18): 2714–2737. doi:10.1002/cne.23812.

Projections from the subparaventricular zone define four channels of output from the circadian timing system

Nina Vujovic, **Joshua J. Gooley**, **Thomas C. Jhou**, and **Clifford B. Saper**

Department of Neurology, Program in Neuroscience, and Division of Sleep Medicine, Harvard Medical School, Beth Israel Deaconess Medical Center, Boston, MA 02215

Abstract

The subparaventricular zone of the hypothalamus (SPZ) is the main efferent target of neural projections from the suprachiasmatic nucleus (SCN) and an important relay for the circadian timing system. Although the SPZ is fairly homogeneous cytoarchitecturally and neurochemically, it has been divided into distinct functional and connectional subdivisions. The dorsal subdivision of the SPZ (dSPZ) plays an important role in relaying signals from the SCN controlling body temperature rhythms while the ventral subdivision (vSPZ) is critical for rhythms of sleep and locomotor activity (Lu et al., 2001). On the other hand, the medial part of the SPZ receives input mainly from the dorsomedial SCN, whereas the lateral SPZ receives input from the ventrolateral SCN and the retinohypothalamic tract (Leak and Moore, 2001). We have therefore investigated whether there are corresponding differences in efferent outputs from these four quadrants of the SPZ (dorsolateral, ventrolateral, dorsomedial and ventromedial) by a combination of anterograde and retrograde tracing. We found that while all four subdivisions of the SPZ share a similar backbone of major projection pathways to the septal region, thalamus, hypothalamus, and brainstem, each segment of the SPZ has a specific set of targets where its projections dominate. Furthermore, we observed intra-SPZ projections of varying densities between the four subdivisions. Taken together, this pattern of organization suggests that the circadian timing system may have several parallel neural outflow pathways that provide a road map for understanding how they subserve different functions.

Graphical Abstract

Address correspondence to: Dr. C. B. Saper, Dept. of Neurology, Beth Israel Deaconess Medical Center, 330 Brookline Avenue, Boston, MA 02215; csaper@bidmc.harvard.edu.

Conflict of interest

The authors have no conflicts of interest to disclose.

Role of authors

All authors had full access to all the data in the study and take responsibility for the integrity of the data and the accuracy of the data analysis. Role of authors:

Study concept and design: NV, CBS

Acquisition of data: NV, JJG, TCJ

Drafting of manuscript: NV

Critical revision of manuscript for important intellectual content: CBS, JJG, TCJ

Statistical analysis: not applicable

Obtained funding: CBS, NV

Administrative, technical and material support: TCJ, JJG (and non-authors mentioned in acknowledgements section above)

Study supervision: CBS

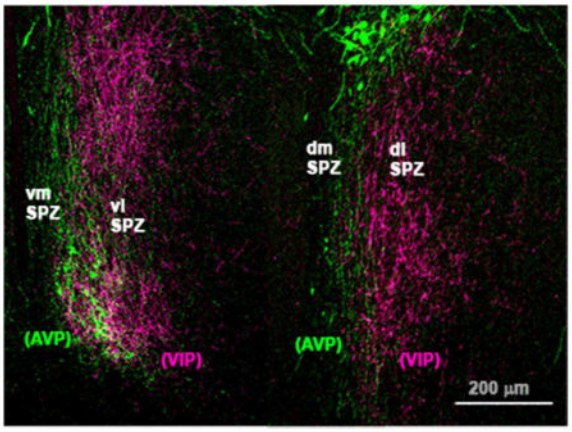

The subparaventricular zone (SPZ) has medial vs. lateral subdivisions, defined by vasopressin (AVP) vs. vasoacitve intestinal peptide (VIP) input from the suprachiasmatic nucleus. There are also dorsal vs. ventral SPZ subdivisions, which have distinct effects on circadian rhythms. Each of the four SPZ quadrants has distinct efferent output pathways.

Introduction

In mammals, daily rhythms in physiology and behavior are driven by rhythmic outputs from the suprachiasmatic nucleus (SCN) (Moore and Eichler, 1972; Ralph et al., 1990; Fuller et al., 2008). The adjacent subparaventricular zone (SPZ), which receives the bulk of neural efferent fibers from the SCN (Watts et al., 1987; Watts, 1991; Leak and Moore, 2001), is thought to be a critical relay for driving rhythms. Lesions of the SPZ (Lu et al., 2001; Schwartz et al., 2009) or knife cuts through it (Inouye and Kawamura, 1979) dramatically attenuate circadian rhythms of sleep, locomotor activity, body temperature, and multiunit activity of neurons in several other brain regions. Furthermore, multiunit activity in the SPZ has a consistent phase relationship to that in the SCN and to locomotor activity rhythms (Inouye and Kawamura, 1979; Kubota et al., 1981; Sato and Kawamura, 1984; Nakamura et al., 2008), further supporting its involvement in SCN outflow circuitry. Differences in the timing of rhythms of immediate early gene expression in the SPZ of rodents active at different times of day suggest that the SPZ may also determine the behavioral phase driven by the SCN signal, establishing whether the animal is diurnal or nocturnal (Smale et al., 2001; Schwartz et al., 2004; Todd et al., 2012).

Though the SPZ consists of a cytoarchitecturally homogeneous population of neurons, which is almost uniformly GABAergic (Lein et al., 2007), it may have different functional subdivisions. Cell-specific lesions in the more dorsal and caudal half of the SPZ (dSPZ) dramatically reduce the amplitude of the body temperature rhythm, but not locomotor activity and sleep rhythms, while cell loss in the more ventral and rostral portion (vSPZ) significantly correlates with loss of rhythms in activity and sleep/wakefulness, largely sparing the temperature rhythm (Lu et al., 2001). On the other hand, anatomical data suggest that the SPZ may be organized into medial vs. lateral subdivisions. Outputs of the ventrolateral SCN (vlSCN, also called the SCN core or retinorecipient region of the SCN),

which is chiefly responsible for circadian entrainment to light, preferentially innervate the lateral portion of the SPZ, while the dorsomedial SCN (dmSCN, also known as the SCN shell), projects more to the medial portion of the SPZ (Leak et al., 1999; Leak and Moore, 2001; Moore et al., 2002; Aton and Herzog, 2005). The lateral SPZ also receives far more robust direct retinal input, (Johnson et al., 1988; Levine et al., 1991; Costa et al., 1999; Gooley et al., 2003; Canteras et al., 2011), suggesting it may be more closely tied to functions that are sensitive to light levels.

The above observations suggest that the SPZ may have four distinct subregions (dorsal vs. ventral, medial vs. lateral), and we hypothesize that their connections should underlie regional differences in function. Although previous studies have examined SPZ efferents using anterograde tracing in rats (Watts et al., 1987; Deurveilher et al., 2002; Chou et al., 2003; Deurveilher and Semba, 2003; 2005; Canteras et al., 2011) and other species (Morin et al., 1994; Kriegsfeld et al., 2004; Schwartz et al., 2011), none of these have explored differences in projections from these different SPZ subdivisions. We have used a combination of anterograde and retrograde tracing to identify distinct projections from each of the SPZ subregions to provide a map for exploring their functional specificity.

Materials and Methods

Animals and surgery

All protocols used in this study were approved by the Harvard University and Beth Israel Deaconess Medical Center Animal Care and Use Committees and conform to the regulations detailed in the National Institutes of Health *Guide for the Care and Use of Laboratory Animals* The cases analyzed in this study were drawn from a library of several hundred experiments done in the Saper laboratory over a number of years in which injections of anterograde or retrograde tracers were placed in a wide variety of locations in the hypothalamus in rats. Adult male Sprague-Dawley rats weighing 350–400g were obtained from Harlan (Indianapolis, IN, RRID:RGD_737903), and housed individually in a 12:12hour light dark cycle with *ad libitum* access to water and food (Purina rodent chow). Surgeries to inject tracer were performed as described previously (Chamberlin et al., 1998). Briefly, rats were anesthetized with an intraperitoneal injection of either chloral hydrate (350 mg/kg) or ketamine-xylazine (80mg/kg ketamine, 8mg/kg xylazine) and placed in a stereotaxic apparatus (David Kopf Instruments, Tujunga, CA). Under aseptic conditions the brain was exposed and an injection of tracer delivered through a glass micropipette by using a compressed air puff system. The skin was then closed with wound clips and the animals given subcutaneous injections of the analgesic meloxicam (1 mg, daily for two days) or flunixin (1 mg/kg, every 12 hours for two days).

Tracers and coordinates

Retrograde tracing was accomplished using 3–10 nl injections of Cholera toxin subunit B (CTb) (10 μg/μl saline, List Biological, Campbell, CA), whereas anterograde tracing was done using either 3–15 nl injections of 10KDa biotinylated dextran amine (BDA) (125 μg/μl saline, Molecular Probes, Eugene, OR, Cat # N-7167) or 7–20 nl of a solution containing adeno-associated viral vectors (either serotype 2 or 8) bearing a gene for green fluorescent

protein (AAV-GFP), prepared by the Harvard Gene Therapy Initiative Virus Production Core (RRID:nlx_156316) as described previously (Chamberlin et al., 1998). All injections were delivered by air pressure from a fine glass micropipette with a 20 μm diameter tip. Injections were made by puffs of air that gradually injected the tracer over 2–5 minutes. The pipette was then left in place for 10 minutes to limit diffusion up the pipette trace as the pipette was slowly withdrawn. The AAV-GFP vector is prepared from a serotype 2 AAV, which binds locally and selectively transduces neurons near the injection site. The transduced neurons then produce GFP that fills the entire cytoplasmic compartment (including fibers and terminals), without causing inflammatory astrocytic or microglial responses in the surrounding tissue, and with minimal retrograde transport. Animals injected with CTb or BDA were perfused one to two weeks following surgery, but we allowed five to nine weeks between injection of AAV-GFP and perfusion, to ensure adequate filling of the terminals of transduced neurons. All injection coordinates were based on the atlas of Paxinos and Watson (Paxinos and Watson, 2005) and were as follows: VMH (AP −2.2; DV −8.8; RL +0.3), DMH (AP −3.5; DV −8.5; RL +0.5), VLPO (AP +0.4; DV −8.4; RL +0.9), SPZ/SCN (injections placed at 16° angle AP −1.75; DV −8.6; RL +2.6). We also examined brain tissue from rats which received intraocular injections of 4 μl AAV-GFP in a previous study (Gooley et al., 2003).

Tissue Preparation

Following sufficient time after surgery for axonal transport (above), rats were deeply anesthetized with chloral hydrate (500 mg/kg) and transcardially perfused with 0.9% saline followed by 10% neutral buffered formalin (Sigma, RRID:nlx_152460). Brains were removed and postfixed for approximately 3 hours in formalin and then allowed to equilibrate for at least 12 hours in a 20% sucrose solution in phosphate buffered saline with 0.01% sodium azide. Brains were subsequently sectioned at 40 μm on a freezing microtome into five series.

Immunohistochemistry

Immunohistochemistry was performed on floating sections following a protocol described in previous publications (Bruinstroop et al., 2011). Sections were rinsed at least three times for 5–10 minutes in 0.1M phosphate buffered saline (PBS), pH 7.4, for 1 hour, then were incubated in 0.3% hydrogen peroxide to block endogenous peroxidase activity. Following at least three more rinses in PBS, sections were incubated for at least 10 hours at room temperature, on a shaker set to 40 rpm, in a solution containing the appropriate primary antibody (see below) in PBS containing 0.3% Triton X-100 and 0.01% sodium azide. Sections were then rinsed at least three more times in PBS before a one-hour incubation in a corresponding secondary antibody (see below for specific information), rinsed three more times in PBS, and then incubated for 60–90 minutes in an avidin-biotin complex solution (Elite ABC, Vector Laboratories, Cat# PK-6200 RRID:AB_2336826). After three more PBS rinses, the tissue was moved to a solution containing 1% 3,3′-diaminobenzidine (DAB) and reacted with 0.01% hydrogen peroxide to visualize the sites containing antigen in the tissue. Once the desired staining intensity was reached, this reaction was quenched with several rinses of the tissue in a PBS solution containing 0.01% sodium azide. Sections were then mounted onto gelatin coated glass slides and allowed to dry overnight at room temperature.

This was followed in some cases by silver-gold enhancement and/or counterstaining with thionin. Silver-gold enhancement consisted of a 30 – 45 minute incubation of desalinated slides in 1% silver nitrate solution at 56 °C, followed by three rinses with water, a 10–20 minute incubation in 0.1% gold chloride, three more rinses and a brief treatment with 5% sodium thiosulfate solution until the tissue reached the desired background level. All slides were rinsed in distilled water before they were dehydrated in graded alcohols and then cleared in xylene for at least 2 hours and cover-slipped with Permaslip medium (Alban Scientific, St. Louis, MO). Counterstained sections were incubated briefly in thionin solution and differentiated in acid alcohol prior to dehydration.

Neurons labeled with the AAV-GFP vector were visualized with a primary antibody against GFP (Molecular probes/Invitrogen ca# A6455, RRID:AB_221570, Lot# 771568), used at a concentration of 1:20,000 followed by biotinylated donkey anti-rabbit secondary (Jackson Immunoresearch Laboratories Cat# 711-065-152, RRID:AB_2333077) used at a 1:1,000 dilution. Tissue from cases injected with BDA underwent the same steps in the avidin-biotin staining protocol, except did not require primary or secondary antibodies. For retrograde tracing cases, immunohistochemistry was done with a primary antibody against CTb raised in goat (List Biologicals, Cat# 703, RRID:AB_10013220), used at a 1:25,000 dilution, followed by a biotinylated donkey anti-goat secondary (Jackson Immunoresearch Laboratories, Cat# 705-065-003, RRID:AB_2340396) used at a 1:1,000 dilution.

For AVP/VIP double fluorescent immunolabeling, brains were used from a transgenic line of rats which expressed an AVP-eGFP fusion protein from the AVP locus (Ueta et al., 2008), a generous gift from the laboratory of Dr. Charles Allen, were stained for VIP, and GFP signal in AVPergic cells was amplified immunohistochemically. Tissue was incubated for two nights with a polyclonal primary antibody raised in rabbit against synthetic VIP coupled to bovine thyroglobulin with a carbodiimide linker (ImmunoStar, Cat# 20077, RRID:AB_572270, Lot: 722001) at a concentration of 1:1,000 and a monoclonal primary antibody raised in mouse against Aquaphora GFP protein (Molecular probes/Invitrogen ca# A11120, RRID:AB_221568, Lot# 71C1-1), used at a concentration of 1:500. After incubation with primary antibodies, tissue was taken through six 3-minute long PBS rinses, prior to incubation with a pre-adsorbed biotinylated donkey anti-rabbit secondary (Jackson Immunoresearch Laboratories Cat# 711-065-152, RRID:AB_2333077). This secondary antibody, at a 1:100 concentration, was pre-adsorbed for 1 hour with a solution of rat brain powder to decrease non-specific background labeling. This powder was prepared from formalin-fixed rat brains as described previously (Standaert et al., 1986). The solution was then centrifuged, and only the supernatant was incubated with tissue for immunolabeling. Following this 1-hour incubation, tissue was rinsed five times for three minutes, then incubated for 30 minutes in a solution containing an Alexa 488-tagged donkey anti-mouse secondary antibody (Molecular Probes/Invitrogen Cat# A21202, RRID:AB_141607), used at 1:500, and a Cy-3-tagged mouse anti-biotin antibody (Jackson Immunoresearch Laboratories, Cat# 200-162-211, RRID:AB_2339026) used at 1:500. Rinsed tissue was mounted onto slides and allowed to dry in a darkened chamber before it was cover-slipped with Dako fluorescent mounting medium (Dako, Carpinteria, CA).

Antibody characterization

Please see Table 1 for a list of all antibodies used:

- The CTb primary antibody used to visualize retrogradely labeled neurons (List Biologicals, Cat# 703, RRID:AB_10013220) does not stain anything above background level in tissue from animals not injected with CTb.
- The GFP primary antibody used to label neurons injected with the AAV-GFP vector (Molecular probes/Invitrogen ca# A6455, RRID:AB_221570, Lot# 771568) did not stain anything in tissue from uninjected animals.
- The GFP primary antibody used to amplify intrinsic GFP signal in AVP-eGFP rat tissue (Molecular probes/Invitrogen ca# A11120, RRID:AB_221568, Lot# 71C1-1) did not stain anything in wildtype rat brains.
- The specificity of VIP primary antibody (ImmunoStar, Cat# 20077, RRID:AB_572270, Lot: 722001) was validated by preadsorption with VIP (which abolished staining) vs. related peptides (which did not), as described in the manufacturer's technical information. Patterns of VIP labeling in the SCN and proximal areas also matched that reported in previous publications (Hattar et al., 2006; Belenky et al., 2008).

Analysis, illustration and photography

Slides were examined and brightfield/darkfield photomicrographs were acquired with a Zeiss Axioplan 2 microscope using Axiovision software (Carl Zeiss, RRID:SciRes_000111), and a 1.5 megapixel color Evolution MP camera (MediaCybernetics, Bethesda, MD). Detailed cytoarchitectonics of DAB-stained target regions were delineated by co-staining sections labeled for the tracer with a Nissl marker. Each section was carefully examined at 10x magnification in darkfield. Boundaries of target regions and their sub-regions were determined by matching borders delineated by Nissl staining to those at corresponding brain levels in the Paxinos and Watson (2005) rat brain atlas. Dual labeling immunofluorescence images were acquired using a Zeiss LSM 510 confocal microscope (BIDMC Confocal Imaging Core, RRID:SciEx_11637) and processed using ImageJ software (National Center for Microscopy and Imaging Research: ImageJ Mosaic Plug-ins, RRID:nif-0000-10512, National Institutes of Health, Bethesda, MD USA). All images were then processed with Adobe Photoshop software (Adobe Photoshop CS2, RRID:SciRes_000161) to optimize the brightness/contrast. Red fluorescence was shifted to magenta in some images to make the difference from green visible to viewers with red-green color-blindness (Fig. 1A–C) and in images of DAB-stained injection sites (e.g. Fig. 1G), red, orange, and yellow hues were partially desaturated to distinguish between the injection site and fibers radiating at high density from it. Illustrations of injection sites and anterogradely labeled fibers were made using a Leitz Wetzlar camera lucida attachment on a Leitz LaborluxS microscope (Leitz, Germany). These drawings were digitized using a Wacom Intuos PTK-1240 tablet (Wacom Co., Saitama, Japan) and Adobe Illustrator Software (Adobe Systems, San Jose, CA, USA, Adobe Illustrator CC, RRID:nlx_157287).

Results

SCN and retinal afferents to the SPZ define its medial and lateral subdivisions

The SPZ is defined by the dense terminal area occupied by axons from the SCN (Watts et al., 1987) rather than by a characteristic cytological pattern. In Nissl-stained sections it is not possible to divide the SPZ into regions, or even to differentiate it from the rest of the periventricular nucleus or anterior hypothalamic area. For these reasons we have used the inputs to the SPZ from the retina and the SCN to clarify its medial vs. lateral organization and to designate the regions we will refer to as the dorsomedial (dmSPZ), dorsolateral (dlSPZ), ventromedial (vmSPZ) and ventrolateral (vlSPZ) components of the SPZ in our subsequent analysis.

To visualize SPZ inputs from both major SCN subregions, we took tissue from rats in which cells containing arginine vasopressin (AVP), a marker for many neurons in the dmSCN, have been genetically engineered to natively express green fluorescent protein (Ueta et al., 2008) and labeled it with an antiserum against vasoactive intestinal polypeptide (VIP), a marker for many neurons in the vlSCN (Leak and Moore, 2001, Moore et al. 2002) (see Fig. 1A–C). AVP and VIP positive fibers course dorsally and caudally from the SCN, with the densest region of immunoreactive fibers and terminals defining the SPZ. VIP-immunoreactive fibers and terminals in the SPZ are densest in the more lateral aspects of the SPZ, and rarely are found in the 100 μm or so along the edge of the third ventricle. AVP-immunoreactive fibers, on the other hand, course through the more medial aspect of the SPZ, closer to the wall of the third ventricle, but are rarely found in the most lateral 150 μm or so of the territory marked by the VIP axons. The two fiber groups overlap in the middle 150 μm or so of the SPZ. The source of these VIP fibers is unambiguous, as there are no other major VIP-expressing cell groups or fiber pathways in the hypothalamus. Although there are other AVP cell groups in the region (in the periventricular and paraventricular nuclei), previous work has demonstrated that AVP-immunoreactive fibers in the SPZ are also derived from the SCN, as they are lost following SCN lesions (Kalsbeek et al., 1993).

To confirm that the trajectory of the AVP-immunoreactive axons identifies the pathway from the entire dmSCN, we also placed an injection of AAV-GFP selectively into the dmSCN (Fig. 1G–I) of a wildtype rat. Fibers and terminals originating non-specifically in the dmSCN, like the SCN AVP axons, ran medially along the third ventricle and extending out laterally to cover all of the medial SPZ, but avoiding the most lateral one-fourth of the SPZ. In both types of experiments, more axonal ramification was seen laterally at intermediate levels of the SPZ (Fig. 1B, H) than at the most rostral/ventral or caudal/dorsal levels. In a case in which AAV-GFP had been injected into the eye (as described in Gooley et al., 2003), the labeled retinal axons mainly occupied the lateral part of the ventral SPZ (see Fig. 1D–F). Based on the above findings, we therefore identify the SPZ in rats as a zone about 400μm wide extending dorsally and caudally from the SCN along the third ventricle, in which the medial half is dominated by dmSCN input and the lateral half by vlSCN and retinal input. Furthermore, there is an exclusive area, about 100 μm wide on the medial, and 150 μm wide on the lateral side of the SPZ that receives input almost exclusively from the

medial or lateral pathway, respectively, with a zone of overlap of about 150 μm in the center of the SPZ.

Our delineation of the SPZ and its subdivisions was also influenced by the results of cell-specific lesion studies (Lu et al., 2001), which showed that the dorsal and ventral parts of the SPZ play distinct roles in transmitting different SCN-driven circadian rhythms. Hence, we divided the SPZ, based upon those physiological findings and the extent of retinal input, into a ventral zone extending about 600μm dorsally and caudally from the border of the SCN and a dorsal zone, extending about 600μm ventrally and rostrally from the border of the paraventricular nucleus.

This description of the SPZ differs in subtle ways from that set forth by Watts (1991), who, for example, considered the most medial part of the SCN projection zone to be part of the periventricular nucleus rather than the SPZ. Because we could not see a distinction here in the pattern of axon termination, we chose to include it in the SPZ. On the other hand, Watts' SPZ extends slightly further caudally and ventrally (to hug the dorsomedial boundary of the ventromedial nucleus of the hypothalamus). We did not include this caudal extent of the SCN projection because it continues on into the ventromedial and dorsomedial nuclei, and there is no physiological evidence that the SPZ cells in the region surrounding these nuclei contribute to circadian rhythms. Watts also shows the SPZ including cells along the lateral boundary of the SCN. We did not include that region because axons from neither the AVP- nor VIP-immunoreactive axons from the SCN terminate there.

Location of anterograde tracer injections in the subparaventricular zone

Twenty-four cases in our collection had injections that included at least some part of the SPZ. We selected ten AAV-GFP injections and two BDA injections placed most focally within the SPZ for analysis of SPZ subregion targets (Fig. 2).

In case 2569 (Fig. 2A), the injection was placed in the **vlSPZ**. This injection filled most of the vlSPZ and involved little else, although a few neurons along the dorsal margin of the SCN were included. In case NVA84 (Fig. 2A), the injection was placed into the **vmSPZ**, extending laterally to include a part of the vlSPZ and just a few cells along the dorsal surface of the dmSCN, but did not include the most dorsal aspect of the vmSPZ. In cases NVA36 and NVA37 (Fig. 2A), the injections predominantly involved vmSPZ neurons, but extended considerably further into adjacent areas than NVA84. However, they did confirm the projection pattern from the vmSPZ as identified in NVA84.

In cases 2567 (Fig. 2B) and NVA140 (Fig. 2C), the injections were confined to the **dlSPZ**, while the injection sites in cases NVA44 (Fig. 2C) and NVA144 (Fig. 2B) included both dlSPZ as well as some adjacent cells in parts of the anterior hypothalamic area that receive few direct SCN efferents. In case NVA64 (Fig. 2B), the injection was placed selectively in the **dmSPZ**, whereas in cases NVA22, NVA21 (Fig. 2C) and NVA142 (Fig. 2C) the injections included dmSPZ neurons as well as a few neurons in the paraventricular nucleus of the hypothalamus (PVH). We found no major differences in projections labeled by comparable injections using AAV-GFP (e.g., NVA140) vs. BDA (Case 2567) except that AAV-GFP often provided better filling of axons innervating the most distal targets.

Efferent projections from the subparaventricular zone

We found that although the backbone of major output pathways was similar after injections in each quadrant of the SPZ, there were substantial differences in the patterns of terminal areas that were innervated. Most of these projections were similar to earlier descriptions (Watts and Swanson, 1987; Morin et al., 1994; Kriegsfeld et al., 2004; Deurveilher and Semba, 2005), but some of the longer projections (e.g., to the amygdala and brainstem) had not been previously reported, nor had the regional origin of these projections within the SPZ been appreciated. To put these into perspective and to provide a background for considering the specific origins of particular projections, we first provide an overall description of the backbone pathways from which the terminal fields emerge (based on case NVA36). Although the injection in this case was centered in the vmSPZ, it also included parts of the adjacent vlSPZ and dmSPZ. More importantly, all of the common major pathways that were labeled in the other experiments were seen in this example (Fig. 3). We will then focus on the differences between the most densely labeled terminal areas after injections in specific quadrants of the SPZ.

It is convenient to describe the projections labeled in case NVA36 based on the four major directions of outflow, rostral, dorsal, caudal and lateral. Most projections were predominantly on the ipsilateral side of the brain, with a much smaller number of axons forming a similar pattern on the other side of the brain, although a few sites identified below had more extensive contralateral projections. These appeared to cross the midline mainly as part of the ventral supraoptic commissure.

Rostral projections—This group of axons richly innervated the rostral periventricular nucleus, medial and median pre-optic nuclei and to a lesser extent, the anterior hypothalamic area (Fig. 3B, C). Fibers continued rostrally to provide a dense terminal field in the anteroventral periventricular nucleus and the ventromedial preoptic nucleus (Fig. 3B). Slightly less dense innervation was present in the adjacent ventrolateral preoptic nucleus and relatively few fibers are seen further laterally in the nucleus of the horizontal limb of the diagonal band, the ventral pallidum, and the substantia innominata (Fig. 3A, B). A considerably heavier group of fibers coursed anterodorsally, many of them hugging the ventral boundary of the anterior commissure, with some terminating in the parastrial nucleus. Many fibers from this trajectory continued anterodorsally to terminate in the bed nucleus of the stria terminalis, the lateral septal nucleus (chiefly in the ventral subdivision of this nucleus), and a few in the medial septal nucleus (Fig. 3A, B).

A distinct subpopulation of fibers in the rostral pathway diverged from the rest at approximately the level of the optic chiasm and coursed dorsolaterally in a diagonal path to merge with the stria terminalis. These fibers terminated in the medial nucleus, and to a lesser extent the central nucleus of the amygdala (Fig. 3E–G).

Dorsal projections—This outflow pathway from the SPZ was the most robust. Fibers coursed from the injection site dorsally along the third ventricle to the foramen of Monro, where they turned caudally to innervate the paraventricular nucleus of the thalamus (PVT) (Fig. 3C–F). At more caudal SPZ levels, smaller numbers of axons penetrated the

paraventricular nucleus of the hypothalamus and thalamic reuniens nucleus (which they sparsely innervated), to reach the PVT (Fig. 3C–E). Some axons left the PVT laterally to form boutons in the paratenial nucleus of the thalamus or in the lateral habenular nucleus (Fig. 3F). The PVT was one of the SPZ's most densely innervated targets, receiving SPZ projections along its full rostrocaudal extent, with the densest projection targeting the rostral aspect of this nucleus on the side ipsilateral to the injection site (Fig. 3C–F).

Caudal projections—The pathway from the SPZ to more posterior hypothalamic structures and ventromedial midbrain targets was also one of its most robust outputs, and as will be discussed later, axons from different SPZ subregions innervated specific targets. The axons in this pathway coursed caudally along the wall of the third ventricle, providing variable amounts of innervation to the ventromedial (VMH) and dorsomedial (DMH) hypothalamic nuclei (Fig. 3E, F). In case NVA36, there was an exceptionally dense cluster of fibers and boutons around the capsule and perimeter of the VMH and in one segment of the central subdivision of the nucleus, but comparatively sparser innervation to the dorsomedial, or ventrolateral divisions (Fig. 3F). Many fibers coursed along the medial and ventromedial edge of the VMH, filling the internuclear space between it and the DMH, the periventricular nucleus, and the arcuate nucleus, and innervating these adjacent structures as well. In case NVA36 the DMH received moderate innervation (Fig. 3F) throughout its rostrocaudal extent, which was densest in the medial portion of this nucleus and tapered toward its lateral edge. Input to the arcuate nucleus was largely confined to its lateral portion and was denser at caudal levels of the nucleus. Case NVA36 showed a very rich input to the median eminence (Fig. 3E), with a dense terminal field in both the internal and external laminae ipsilaterally and a fairly dense plexus of boutons and fibers in only the external lamina contralaterally. Fibers continued caudally to the premammillary, medial mammillary, and supramammillary nuclei with the latter showing greater bilateral symmetry than other targets (Fig. 3G, H). Fibers also extended ventrally to line the ventral edge of the mammillary body itself. At the premammillary level, a subset of caudal pathway axons projected posterolaterally with a few fibers curving ventrally to terminate in the ventral tuberomammillary nucleus (Fig. 3G), while others joined the ventral supraoptic commissure fibers to run along the medial border of the optic tract, giving rise to a terminal field in the thalamic intergeniculate leaflet (Fig 3G, 4B).

The remainder of the fibers in the caudal pathway flowed dorsomedially through the posterior hypothalamic area into the central gray matter and Edinger-Westphal nucleus (Fig. 3G, K). Occasional fibers from the periaqueductal gray matter ended on nearby caudal targets, such as the dorsal raphe nucleus (Fig. 3K, 4C) or the olivary pretectal nucleus (Fig. 3G, 4A). A small number of fibers traversed the tectum, often passing along the midline between the superior and inferior colliculi (Fig. 3J). As the cerebral aqueduct opened into the fourth ventricle, the fibers in the periaqueductal gray matter provided modest innervation of the lateral parabrachial nucleus (bilaterally), the pre-coeruleus area (ipsilaterally) and a few fibers reached the ipsilateral locus coeruleus and Barrington's nucleus as well (see Fig. 3L, M, 4E, F).

Lateral projections—This outflow from the SPZ was sparser than the rostral, caudal, or dorsal outflow. Axons exiting the SPZ laterally innervated neurons in the anterior and lateral hypothalamic areas (Fig. 3C–F). This projection was bilateral although much denser ipsilaterally. While innervation patterns in the lateral hypothalamus were fairly similar across injection cases, there was considerably more variability in the anterior hypothalamic area, particularly the subregion flanking the SPZ, which varied depending upon placement of the injection in the SPZ (see Table 2). Other laterally-bound fibers first descended ventrally and then coursed laterally along the optic tract in the ventral supraoptic commissure, forming terminals along the way in the retrochiasmatic area and the supraoptic nucleus (Fig. 3C, D). Fibers were present in the ventral supraoptic commissure as it traveled along the medial aspect of the optic tract at all levels bilaterally, and a subset of these, joined by fibers from the posterior pathway gave rise to the small terminal field seen in the intergeniculate leaflet (fig. 4B).

Subparaventricular zone subregions differ most in their intrahypothalamic efferent projections

Whereas the four SPZ subdivisions share many of the features described for case NVA36, each subdivision has a distinct pattern of terminal innervation, particularly in the preoptic area and caudal hypothalamus. These differences are discussed at length below and highlighted in Fig. 5. Table 2 contains a comprehensive, semiquantitative listing of terminal strength for efferent outputs of all four subparaventricular zone subregions.

Ventromedial SPZ—Of all four subregions, the vmSPZ showed the strongest outputs in the rostral and dorsal pathways. Ventral preoptic targets near the midline, including the organum vasculosum of the lamina terminalis, anteroventral periventricular nucleus, median preoptic nucleus, and ventromedial and ventrolateral preoptic nuclei were particularly richly innervated in case NVA84 (Fig. 5E, Table 2). Also, while other subregions sent at least as strong a projection to the medial preoptic area as to the median preoptic nucleus (if not stronger), in case NVA 84 the median preoptic nucleus was preferentially innervated.

The vmSPZ also sent the richest projections dorsally into the anterior portion of the periventricular zone, to the rostral PVT and to the PVH, providing a particularly strong input to the anterior parvicellular PVH. The contralateral input to the PVT was remarkably strong, and contralateral innervation of the anterior PVH was also substantial.

The vmSPZ innervated the ipsilateral SCN and dmSPZ more richly than did any other SPZ subdivision (Fig. 5A, 6C, Table 2). It also provided fairly strong input to the ipsilateral vlSPZ, and an unusually robust projection to the contralateral vmSPZ, extending somewhat into the contralateral vlSPZ as well. The vmSPZ innervated the adjacent anterior and lateral hypothalamic areas and the DMH (Table 2) more heavily than did other SPZ subdivisions. Fibers and boutons in the DMH were densest at its most rostral level and at the level of the compact subdivision (especially the medial third of these). The vmSPZ projection to the VMH was not quite as strong as that from the dlSPZ (Fig. 5I, L), but showed a very distinct spatial pattern, with terminals preferentially innervating the dorsomedial VMH, dorsal and medial aspects of the VMH capsule, the central portion of the VMH, and the internuclear

spaces in between the VMH and the DMH, arcuate nucleus, and periventricular zone (Fig. 5I). The vmSPZ also sent a significantly stronger projection to the median eminence (Fig. 5I) than did the vlSPZ or dlSPZ, although, as described below, not as strong as that of the dmSPZ (Fig. 5K).

Ventrolateral SPZ—The vlSPZ had moderate to strong outflow in all four general pathways, and its distinct features were found in a few individual regions along each pathway. In particular, unlike other SPZ subregions, the vlSPZ preferentially innervated the ventrolateral portion of the VMH (Fig. 5J), making it the only SPZ region whose VMH terminal field became denser the further caudally it went. However, like most subregions, the vlSPZ provided stronger inputs to the capsule of the VMH (and internuclear spaces surrounding it) than to the body of the VMH. The vlSPZ gave rise to a moderate projection to the rostral DMH (Fig. 5F) with slightly less bias toward its medial aspect than seen with vmSPZ projections (Fig. 5I). More caudally, the vlSPZ sent a particularly strong input to the central gray matter and ipsilateral premammillary region, but a fairly weak input to the supramammillary nucleus, and the weakest input to the median eminence of all four SPZ subdivisions (see Table 2). The vlSPZ also strongly innervated the SCN, vmSPZ and dlSPZ, but only sparsely innervated the dmSPZ or any of these structures on the contralateral side of the brain (Table 2, Fig. 6D). Inputs to the amygdala were confined to the ipsilateral medial nucleus, showing no innervation of the central nucleus or the contralateral side.

Dorsomedial SPZ—The dmSPZ includes the portion of the periventricular nucleus which is richly innervated by the dmSCN (Fig. 1). Thus, it is to be expected that projections from this subregion share certain similarities with outputs from the periventricular zone in general. Our experiments demonstrated that this was indeed the case.

Unlike the other SPZ subregions, the dmSPZ did not have a particularly strong dorsal or caudal outflow, the main exception being an intense input to a series of endocrine structures including the external lamina of the median eminence, a somewhat less intense projection through the internal lamina of the median eminence, and a moderate projection to the arcuate nucleus (Fig. 5K), suggesting that the dmSPZ may be a major site for circadian interactions with the endocrine system. Projections to the tuberomammillary, premammillary, supramammillary and medial mammillary nuclei were much less intense, although the subset of fibers terminating along the edges of the mammillary body was as dense after dmSPZ injections as any SPZ subregion. Across all four of our dmSPZ injection cases, the DMH received a more substantial input than the VMH, although neither terminal field was heavy (Fig. 5K). Though not intense at any level, the innervation of the DMH by the dmSPZ was more consistent along the rostro-caudal extent of this nucleus than innervation coming from other SPZ domains.

Inputs from the dmSPZ to the paraventricular thalamus were also sparse (especially to the more posterior portions of this nucleus). In three of our four cases, we could not find labeled fibers in the lateral habenula. The fourth injection included a few labeled neurons in the dlSPZ and PVH, which may account for the very sparse habenular innervation seen. More rostrally, there was a moderate input to the anterior PVT, although not much innervation to the thalamic reuniens nucleus and even less to the paratenial nucleus (see Table 2). The

parvicellular PVH received a substantial projection from the dmSPZ, which preferentially innervated the most rostral and caudal parvicellular subregions of this nucleus (Fig. 5C). Axons from the dmSPZ innervated the magnocellular PVH subdivision less intensely than its parvicellular components, but more extensively than did other SPZ subregions.

Anterior projections from the dmSPZ followed a pattern similar to the vlSPZ but with less intensity. Interestingly, the projection through the stria terminalis and into the amygdala was as intense as that from other SPZ subregions, and terminal fields in the contralateral amygdala were more extensive. Ipsilaterally, we saw a particularly widespread projection to the amygdala with fibers coursing through adjacent structures to terminate predominantly in the medial and central nuclei (Table 2).

Finally the dmSPZ gave rise to a particularly heavy lateral projection, with many fibers following arcing trajectories into the lateral hypothalamus. Some of these labeled axons may have been from displaced vasopressin cells belonging to the PVH and sending their axons in this classic arcing trajectory, which turns back along the surface of the optic tract to run into the median eminence. However, some axons innervated the supraoptic nucleus and others apparently entered the ventral supraoptic commissure. Axons in the lateral pathway also followed the optic tract to the intergeniculate leaflet, as with other cases. The dmSPZ sent a sizeable projection to the vmSPZ and a stronger projection to the retrochiasmatic area than any other SPZ subregion (Table 2, Fig. 6A).

Dorsolateral SPZ—The dlSPZ had robust outputs along all four major output pathways, but preferentially innervated certain structures along each path. Rostrally, the dlSPZ provided the densest input to the bed nucleus of the stria terminalis and substantia innominata (relative to other SPZ subregions). There was also fairly strong input to the diagonal band nuclei and parastrial nucleus (see Table 2). Via the dorsal outflow pathway, it provided a consistently strong input to all rostro-caudal levels of the PVT and a stronger input to the habenula than any other part of the SPZ (Table 2). Fibers in the lateral pathway gave rise to the densest terminal field seen in the anterior hypothalamic area with a less intense extension into the lateral hypothalamic area (Table 2).

Along the caudal pathway, dlSPZ neurons provided an exceptionally dense and uniform terminal field throughout the entire length of the VMH (Fig. 5L, Table 2), most densely innervating the core of the dorsomedial subdivision of the VMH as well as the central subdivision and the internuclear capsular spaces surrounding the VMH. The projection to the DMH was of more modest intensity, distinctly favoring the rostral and medial third of this nucleus (Fig. 5L, Table 2). Axons continued caudally through and lateral to the arcuate nucleus, providing moderate numbers of labeled boutons in the median eminence and the caudal arcuate nucleus. Of all subregions, the dlSPZ gave rise to the densest terminal fields in areas associated with arousal and reward, including the tuberomammillary nucleus, posterior hypothalamus, and ventral tegmental area, with a strong input to the central gray matter as well.

The dlSPZ also provided local projections to the SCN and other SPZ subdivisions. In particular, a heavy field of terminals and ramifications was seen in the ipsilateral vlSPZ, and

vmSPZ. While some terminals were also visible in the dmSPZ and SCN, these were much lower in number.

Retrograde tracing confirms heterogeneity of efferents from different subparaventricular domains

To confirm the validity of differences in anterograde projections to certain targets from the different SPZ subregions, we injected a retrograde tracer (CTb) into four of these target areas: the ventrolateral preoptic nucleus (VLPO), VMH, DMH, and medial ARC (see Fig. 7A, D, G and J, respectively). The four cases described below are exemplars of the patterns of retrograde labeling in the SPZ after particularly well-placed injections.

Ventrolateral preoptic afferents—CTb was injected into the VLPO in case R2059, filling the entire rostro-caudal extent of this nucleus, with densest staining in the ventral VLPO, and extending a bit medially into the ventromedial preoptic area. Retrograde tracing from this site most densely labeled cell bodies in the dmSCN and vmSPZ, but labeled no cells in the vlSPZ (see Fig. 7B). A number of cells were labeled in the dorsal SPZ, mostly around the boundary between the dmSPZ and dlSPZ (Fig. 7C). This is consistent with our anterograde tracing data suggesting that of the sites we analyzed, the vmSPZ is the largest contributor of projections the VLPO (see Fig. 5E, Table 2).

Ventromedial hypothalamic nucleus afferents—After an injection of CTb into the dorsomedial and central subdivisions of the VMH, but including parts of its capsule and a small amount of the ventrolateral VMH in case NVA151, the pattern of retrograde labeling seen in the SPZ was essentially as predicted by our anterograde tracing experiments (see Fig. 5D, L). The dlSPZ, which sends by far the densest projection to the VMH, showed the largest numbers of retrogradely labeled SPZ neurons (Fig. 7E, F). The retrogradely labeled neurons spilled over more laterally into other portions of the anterior hypothalamic area, so it may be more accurate to consider this an anterior hypothalamic projection, the medial portion of which is likely to be influenced by the SCN. The ventral-most (perisuprachiasmatic) portion of the vlSPZ (Fig. 7E) also showed substantial numbers of retrogradely labeled cells although a smaller number of cells than that seen in the dlSPZ. This pattern is consistent with our anterograde injection data showing that the vlSPZ projects predominantly to the ventral portion of the VMH capsule (Fig. 5J). The retrogradely labeled neurons overlapped into the midportion of the ventral SPZ (but not the exclusively medial zone), which explains why the projection to the VMH was also labeled in some of our vmSPZ cases (e.g., Fig. 5I). There was a striking absence of retrogradely labeled cells in the dmSPZ in this case, much as there is a paucity of labeled anterograde projections to the VMH from this region (Fig. 5K).

Dorsomedial hypothalamic nucleus afferents—An injection of CTb was placed in the DMH in case 1927 (Fig. 7G), showing particularly intense filling in the medial third of the rostral DMH but filling the whole rostrocaudal extent of the nucleus. The injection site also spread into the periventricular zone anterior to the DMH, the adjacent lateral hypothalamic area at rostral DMH levels, and to a small portion of the medial posterior arcuate nucleus that lies just caudal and ventral to the DMH. This injection resulted in

labeling of cell bodies along the most medial portion of the SPZ, including mostly cells in the vmSPZ and to some extent in the dmSPZ, with almost no labeling in the vlSPZ (Fig. 7H, I). It seems likely, based on this result, that the dlSPZ injection shown in Fig, 5D labeled axons in the DMH (Fig. 5L) (and which was even heavier in the most caudal portion of the DMH, see Table 2) by including some cells in the middle portion of the dorsal SPZ, along the medial edge of that injection. This result is consistent with retrograde labeling from the DMH previously reported from our lab (Chou et al., 2003).

Arcuate nucleus afferents—In case NVA 150, CTb was injected into the medial portion of the arcuate nucleus and continued dorsally to fill part of the adjacent periventricular zone (Fig. 7J). The injection extended through the rostral and middle levels of the arcuate nucleus, tapering off at the posterior level (just caudal to the VMH). The injection site included the adjacent periventricular zone just dorsal to the arcuate nucleus at rostral levels, extending to the ventral periventricular zone at the level of the retrochiasmatic area. In this case, there was an especially dense cluster of retrogradely labeled cells present in the caudal portion of the vmSPZ (Fig. 7K, L), with scattered retrogradely labeled neurons in the remainder of the SPZ, consistent with our anterograde tracing (see Table 2).

Discussion

Our systematic analysis of SPZ projections indicates that its outputs are organized along both mediolateral and dorsoventral gradients. The four SPZ quadrants each preferentially innervates a distinct set of targets. In addition, the SPZ has several sparse distal projections which have not previously been described, including projections to the dorsal raphe nucleus, locus coeruleus, pre-coeruleus region, lateral parabrachial nucleus and Barrington's nucleus (see Fig. 3, 4 Table 2). We also observed a slightly different and more extensive pattern of innervation than previously described in the amygdala, habenula, and median eminence (see Fig. 3E–G, Table 2). This is also the first study showing that the four SPZ subdivisions project to each other and to the suprachiasmatic nucleus (see Fig. 6, Table 2). This connectivity allows for local circuits to share information within the SPZ and suggests circadian outflow through it could be considerably more complex than previously described.

Technical considerations

The anterograde tracers used for this study, an adeno-associated viral vector expressing GFP (AAV-GFP) and in a few cases biotinylated dextran amine (BDA) have certain strengths and weaknesses: BDA is an excellent anterograde tracer but carries a risk of retrograde uptake and transport anterogradely down collaterals of those same neurons; AAV2-GFP injections of this size rarely cause retrograde labeling of more than one neuron per brain (Chamberlin et al., 1998), hence collateral transport is unlikely to contribute substantially to the projections seen.

Although we used a combination of BDA and AAV-GFP injection cases to analyze differences in SPZ subregion projections, we fortunately have cases with AAV-GFP injections for three out of four SPZ subregions, and are able to compare and verify that injections with the different tracers that are placed in similar sites give rise to extremely similar fiber and terminal fields elsewhere in the brain. The only subregion for which we

must rely on BDA anterograde tracing alone is the vlSPZ. Fortunately, this is a subregion whose efferents have previously been reported using another tracer with less risk for retrograde uptake (*Phaseolus vulgaris* leucoagglutinin, PHAL), and our findings match the previous reports of vlSPZ efferent targets (Canteras et al., 2011).

It is not possible to make rigorous quantitative comparisons of terminal density across two injection cases given the fact that each injection fills a different number and distribution of neuronal cell bodies; we can make only semi-quantitative comparisons across several different cases of injections placed in adjacent/overlapping regions. We have thus relied heavily on case-to-case comparison and complementary retrograde tracing in selected terminal fields to help clarify the differences between projections from different SPZ subdivisions.

Connectivity patterns suggest a role for the ventromedial SPZ in regulation of sleep-wake rhythms

Many of the novel SPZ targets we observed receive the bulk of their input from the vmSPZ and are thought to play a role in sleep/wake regulation, namely the parabrachial nucleus, locus coeruleus, pre-coeruleus region, and dorsal raphe nuclei (Saper et al., 2010). These observations are consistent with earlier studies showing that the ventral SPZ plays a particularly important role in the circadian modulation of sleep (Lu et al., 2001). The vmSPZ also projects more heavily to the lateral hypothalamic area, median preoptic nucleus, VLPO and the DMH than other SPZ subregions (see Table 2). In the case of the VLPO and DMH, we have been able to confirm via retrograde tracing that their SPZ afferents come mostly from the ventromedial quadrant (see Fig. 7) findings which are consistent with those reported previously (Thompson and Swanson, 1998; Chou et al., 2003). While all the sites listed above play significant roles in sleep-wake regulation, only lesions of the DMH specifically disrupt the circadian timing of sleep and wake throughout the day (Chou et al., 2003), suggesting that the vmSPZ projection to the DMH may carry particular functional relevance in circadian modulation of behavioral state.

The vmSPZ also receives an especially strong input from the dmSCN (see Fig. 1G–I), which is preferentially associated with timing of REM sleep rhythms (Cambras et al., 2007). Furthermore, the vmSPZ receives a robust input from each other SPZ subdivision (see Fig. 6), suggesting its output can be modulated indirectly by information relayed through these sites, perhaps enabling circadian regulation of sleep to be modified by light, feeding or other relevant zeitgebers.

Connectivity patterns suggest a role for the medial SPZ in regulation of endocrine rhythms

The dmSPZ is the heaviest source of inputs from the SPZ to the median eminence, followed closely by the vmSPZ. The projections include both the internal lamina, through which AVP axons pass through to the posterior pituitary gland, as well as the external lamina, in which axon terminals secrete pituitary hormone releasing or release-inhibiting hormones into the hypophysial portal system. Thus the SCN output may directly regulate both magnocellular and parvicellular neuroendocrine neurons in the SPZ (Horvath, 1997). The magnocellular neurons are likely to contain AVP, while the parvicellular neurons may secrete dopamine

(which regulates prolactin secretion) or gonadotrophin-releasing hormone (Moore, 1987). Knife cuts through the SPZ are reported to blunt diurnal rhythms of both prolactin and luteinizing hormone (LH) (Watts et al., 1989). In addition to interrupting direct SCN inputs to reproductive endocrine neurons, such knife cuts would also damage relayed inputs. For example, the anteroventral periventricular nucleus (AVPe) is thought to regulate LH release (Robertson et al., 2009) and circadian regulation of LH release is dependent on ipsilateral neural outflow from the dmSCN to the AVPe (de la Iglesia et al., 2003; de la Iglesia and Schwartz, 2006; Smarr et al., 2012). However, there are few direct projections from the dmSCN to the AVPe, and instead this input appears to be mediated by the vmSPZ which both receives a strong input from the dmSCN and sends a robust projection to AVPe.

All four divisions of the SPZ also innervate other sites containing parvicellular neuroendocrine neurons, including the arcuate nucleus and the adjacent periventricular and retrochiasmatic areas (Table 2, Fig. 7) which contains neurons secreting growth hormone releasing factor (Meister et al., 1986), and the paraventricular nucleus, which contains neurons that produce corticotrophin releasing hormone, thyrotropin releasing hormone, and somatostatin (Sawchenko and Swanson, 1982; Lechan et al., 1983; Cole and Sawchenko, 2002). However, the integrity of circadian rhythms of corticosteroid secretion depend upon relays through the dorsomedial nucleus, which receives circadian input from both the SCN and the vmSPZ (Chou et al., 2003). Our observations are consistent with those of Watts and Swanson that the direct SCN projections to the DMH and PVH are considerably weaker than SPZ projections to either region (Watts and Swanson, 1987; Watts, 1991). Hence, the corticosteroid rhythms are likely to depend on the vmSPZ relay to the DMH (Chou et al, 2003).

Finally, the arcuate nucleus contains pro-opiomelanocortin neurons that inhibit feeding and promote caloric expenditure, as well as neurons containing neuropeptide Y and agouti-related peptide that promote feeding and inhibit caloric expenditure (Elias et al., 1998). The SPZ may likewise influence circadian rhythms of these functions either by direct inputs to the arcuate neurons that regulate feeding behavior and energy expenditure, and their responses to leptin and ghrelin (Cone, 2005; Krashes et al., 2011; Kong et al., 2012), or via relays, such as from the dorsomedial nucleus (Chou et al, 2003).

Connectivity patterns suggest the dorsolateral SPZ may modulate behavior and act as an entry point for energy homeostasis zeitgebers

The dlSPZ has extensive reciprocal connections with the VMH, which may have a variety of physiological implications. Our data indicate that the dlSPZ provides a particularly intense input to the dorsomedial VMH (Table 2, Fig. 5, Fig. 7). The dlSPZ also receives a strong input from leptin-sensitive neurons in the dorsomedial VMH (Elmquist et al., 1998). These dorsomedial VMH neurons are implicated in energy homeostasis and maintenance of plasma glucose levels (Tong et al., 2007; Hawke et al., 2009; Xu et al., 2010). The dlSPZ also appears to have fairly robust reciprocal connections with the vmSPZ and vlSPZ (Table 1, Fig. 6), raising the possibility that it relays hunger/satiety cues as a zeitgeber to the rest of the SPZ.

The dlSPZ also has a particularly impressive projection to the ventrolateral VMH (Table 2, Fig. 5, 7), an area implicated in control of aggression and reproductive behavior (Lin et al., 2011). Our anterograde tracing suggests that the dlSPZ may also be the strongest contributor of SPZ projections to the bed nucleus of the stria terminalis and ventral tegmental area (Table 2), which suggests it may be involved in circuitry integrating brain responses to certain kinds of threat and reward.

Taken together, the above findings are consistent with the possibility that the dlSPZ would play a role in scenarios where animals must change their daily behavioral patterns/schedules to avoid predation or other environmental threats, to ensure access to a food source, or to reproduce and effectively care for their young. This intriguing possibility remains to be tested.

Connectivity patterns suggest a role for the ventrolateral SPZ in photic and exercise-mediated entrainment

Of the four SPZ subdivisions, the vlSPZ receives the largest share of input from the retina (Gooley et al., 2003; Canteras et al., 2011), the retinoreceptive vlSCN, and the intergeniculate leaflet (Moga and Moore, 1997; Morin and Blanchard, 1999), which is an area implicated in photic and exercise-mediated resetting of circadian phase (Harrington and Rusak, 1986; Harrington, 1997).

The vlSPZ also projects to the intergeniculate leaflet more robustly than other SPZ subdivisions (see Table 1). Although two previous studies placed the origin of this projection in the retrochiasmatic area and anterior hypothalamus in rats (Moore and Card, 1994) and hamsters (Morin and Blanchard, 1999), it is clear from the drawings by Moore and Card that most of these neurons in rats were adjacent to and just dorsal to the SCN, in what we call the vlSPZ. Morin and Blanchard did not provide a graphical depiction of cells retrogradely labeled from the intergeniculate leaflet, but their description suggests these cells may reside in what we would consider the hamster equivalent of the rat vlSPZ.

In addition to being the SPZ subdivision that projects most strongly to the intergeniculate leaflet, the vlSPZ also projects intensely to the vmSPZ, and dlSPZ, making it well positioned to integrate photic and activity-based entrainment cues into circadian outflow circuitry. Previous studies have suggested that light masking of various rhythms can still occur following damage to the SCN (Redlin and Mrosovsky, 1999) or knife cuts between the SCN and SPZ (Watts et al., 1989), but not following SCN lesions which extend into the adjacent ventral subparaventricular zone (Li et al., 2005). These findings suggest that light masking of activity could be mediated through direct or relayed retinal inputs to the vlSPZ and its downstream outputs. Studies of nocturnal vs. diurnal rodents also indicate that retinal innervation of the vlSPZ (or lack thereof) between postnatal day 8 and 15 coincides with the development of consolidated night-time vs. day-time wakefulness, respectively, and may explain how a rodent’s active phase is established (Todd et al., 2012).

Summary

Outputs from each of the four SPZ subdivisions define a set of distinct domains, which are critically important for organization of circadian and diurnal rhythms of specific functions,

and how they adapt to new schedules. Our results, taken together with previous literature (Watts, 1991; Gooley, 2005) suggest particular roles for the subpopulations of neurons in this region, which in many ways parallel the organization of the SCN and act as its critical relays, but also allow for a secondary level of integration of its outputs.

The medial SPZ may be key in circadian regulation of endocrine function, with the vmSPZ also regulating rhythms in sleep and wakefulness, and perhaps driving circadian variation in REM sleep. The lateral SPZ subdivisions on the other hand, in addition to relaying SCN signals, may act as an entry point for non-SCN inputs, integrating signals from these sites into the circadian outflow circuits. Our findings suggest the vlSPZ is involved in photic and exercise-mediated entrainment of circadian rhythms, and can relay this input to other SPZ subdivisions, while the dlSPZ may be more involved in food and social entrainment and regulation of daily patterns in aggressive and reproductive behaviors through its projection targets.

Acknowledgments

We are grateful to Quan Ha for superb technical assistance throughout this study and to Dr. Charles Allen (and members of his laboratory at OHSU) for generously providing us with AAV-GFP reporter rat brains. We also thank Dr. Ningshan Wang for assistance with confocal microscopy, Ashley Schomer and Peagan Lin for assistance with histology, and Dr. Veronique van der Horst for thoughtful input at various stages of this project. This work was supported by USPHS grants NS072337, AG09975 awarded to C. Saper and the F31 NS071890-03 and NSFGRFP fellowships awarded to N. Vujovic.

Table of Neuroanatomical Abbreviations

3	oculomotor nucleus
3PC	oculomotor nucleus, parvicellular part
AA	anterior amygdaloid area
ac	anterior commissure
AHA	anterior hypothalamic area
AHiAL	amygdalohippocampal area, anterolateral part
ARC	arcuate nucleus of the hypothalamus
AVPe	anteroventral periventricular nucleus
Bar	Barrington’s nucleus
BLA	basolateral nucleus of the amygdala
BMA	basomedial nucleus of the amygdala
BSM	bed nucleus of the stria terminalis, medial subdivision
BST	bed nucleus of the stria terminalis
CeA	central nucleus of the amygdala
CG	central gray
CLi	caudal linear nucleus of the raphe

CnF	cuneiform nucleus
CoA	anterior cortical amygdaloid nucleus
CoApl	posterolateral cortical amygdaloid nucleus
CoApm	posteromedial anterior cortical amygdaloid nucleus
CP	cerebral peduncle
CPu	caudate putamen
DBB	diagonal band of Broca
DHA	dorsal hypothalamic area
Dk	nucleus of Darkschewitsch
dLG	dorsal lateral geniculate nucleus of the thalamus
DMH	dorsomedial nucleus of the hypothalamus
dlSPZ	dorsolateral subparaventricular zone
dmSCN	dorsomedial suprachiasmatic nucleus
dmSPZ	dorsomedial subparaventricular zone
DR	dorsal raphe nucleus
dSPZ	dorsal subparaventricular zone
EW	Edinger-Westphal nucleus
FR	fasciculus retroflexus
f	fornix
GP	globus pallidus
HDB	horizontal limb of the diagonal band
IC	internal capsule
LC	locus coeruleus
InC	interstitial nucleus of Cajal
IPAC	interstitial nucleus of the posterior limb of the anterior commissure
IPN	interpeduncular nucleus
LA	lateral amygdaloid nucleus
LDT	laterodorsal tegmentum
LHA	lateral hypothalamic area
LHb	lateral habenular nucleus
LM	lateral mammillary nucleus
LPB	lateral parabrachial nucleus

LPBel	lateral parabrachial nucleus, externolateral
LPBS	lateral parabrachial nucleus, superior
LPO	lateral preoptic area
LS	lateral septal nucleus
LSv	lateral septal nucleus, ventral part
MCPO	magnocellular preoptic nucleus
Me5	mesencephalic trigeminal nucleus
MeA	medial nucleus of the amygdala
ME	median eminence
MGN	medial geniculate nucleus of the thalamus
MHb	medial habenular nucleus
MLF	medial longitudinal fasciculus
MM	medial mammillary nucleus
MnPO	median pre-optic area
Mo5	motor trigeminal nucleus
MPB	medial parabrachial nucleus
MPO	medial pre-optic area
MPT	medial pretectal nucleus
MR	median raphe nucleus
MS	medial septal nucleus
mt	mammillothalamic tract
NLOT	nucleus of the lateral olfactory tract
NPC	nucleus of the posterior commissure
OX	optic chiasm
OLT	olfactory tubercle
OPT	olivary pretectal nucleus
OT	optic tract
OVLT	organum vasculosum of the lamina terminalis
PAG	periaqueductal gray
PBG	parabigeminal nucleus
PC	posterior commissure
Pe	periventricular hypothalamic nucleus

PIL	posterior intralaminar nucleus of the thalamus
PMD	premammillary nucleus, dorsal part
PMV	premammillary nucleus, ventral part
Po	posterior thalamic nuclear group
PP	peripeduncular nucleus
Pr5	principal sensory trigeminal nucleus
PS	parastrial nucleus
PTA	pretectal area
PVH	paraventricular nucleus of the hypothalamus
PVT	paraventricular nucleus of the thalamus
PIR	piriform cortex
RCh	retrochiasmatic area
Re	nucleus reuniens of the thalamus
SCN	suprachiasmatic nucleus
SCol	superior colliculus
SCP	superior cerebellar peduncle
SFI	septofimbrial nucleus
SI	substantia innominata
SLD	sublaterodorsal nucleus
sm	stria medullaris
SN	substantia nigra
SNc	substantia nigra pars compacta
SNr	substantia nigra pars reticulata
STN	subthalamic nucleus
SO	supraoptic nucleus
SOC	superior olivary complex
SUM	supramammillary nucleus
ST	stria terminalis
TMN	tuberomammillary nuleus
vlSPZ	ventrolateral subparaventricular zone
vmSPZ	ventromedial subparaventricular zone
VDB	vertical limb of the diagonal band

vLG	ventral lateral geniculate nucleus of the thalamus
vlSCN	ventrolateral suprachiasmatic nucleus
VLPO	ventrolateral pre-optic nucleus
VMH	ventromedial hypothalamic nucleus
VMHc	ventromedial hypothalamic nucleus, central part
VMHdm	ventromedial hypothalamic nucleus, dorsomedial part
VMHvl	ventromedial hypothalamic nucleus, ventrolateral part
VMPO	ventromedial pre-optic area
VP	ventral pallidum
VPL	ventral posterolateral thalamic nucleus
VPM	ventral posteromedial thalamic nucleus
vSPZ	ventral subparaventricular zone
VTA	ventral tegmental area
ZI	zona incerta

References

Aton SJ, Herzog ED. Come together, right…now: synchronization of rhythms in a mammalian circadian clock. Neuron. 2005; 48(4):531–534. [PubMed: 16301169]

Belenky MA, Yarom Y, Pickard GE. Heterogeneous expression of gamma-aminobutyric acid and gamma-aminobutyric acid-associated receptors and transporters in the rat suprachiasmatic nucleus. The Journal of comparative neurology. 2008; 506(4):708–732. [PubMed: 18067149]

Bruinstroop E, Cano G, Vanderhorst VG, Cavalcante JC, Wirth J, Sena-Esteves M, Saper CB. Spinal projections of the A5, A6 (locus coeruleus), and A7 noradrenergic cell groups in rats. The Journal of comparative neurology. 2011

Cambras T, Weller JR, Angles-Pujoras M, Lee ML, Christopher A, Diez-Noguera A, Krueger JM, de la Iglesia HO. Circadian desynchronization of core body temperature and sleep stages in the rat. Proceedings of the National Academy of Sciences of the United States of America. 2007; 104(18): 7634–7639. [PubMed: 17452631]

Canteras NS, Ribeiro-Barbosa ER, Goto M, Cipolla-Neto J, Swanson LW. The retinohypothalamic tract: comparison of axonal projection patterns from four major targets. Brain research reviews. 2011; 65(2):150–183. [PubMed: 20863850]

Chamberlin NL, Du B, de Lacalle S, Saper CB. Recombinant adeno-associated virus vector: use for transgene expression and anterograde tract tracing in the CNS. Brain research. 1998; 793(1–2):169–175. [PubMed: 9630611]

Chou TC, Scammell TE, Gooley JJ, Gaus SE, Saper CB, Lu J. Critical role of dorsomedial hypothalamic nucleus in a wide range of behavioral circadian rhythms. The Journal of neuroscience: the official journal of the Society for Neuroscience. 2003; 23(33):10691–10702. [PubMed: 14627654]

Cole RL, Sawchenko PE. Neurotransmitter regulation of cellular activation and neuropeptide gene expression in the paraventricular nucleus of the hypothalamus. The Journal of neuroscience: the official journal of the Society for Neuroscience. 2002; 22(3):959–969. [PubMed: 11826124]

Cone RD. Anatomy and regulation of the central melanocortin system. Nature neuroscience. 2005; 8(5):571–578. [PubMed: 15856065]

Costa MS, Santee UR, Cavalcante JS, Moraes PR, Santos NP, Britto LR. Retinohypothalamic projections in the common marmoset (Callithrix jacchus): A study using cholera toxin subunit B. The Journal of comparative neurology. 1999; 415(3):393–403. [PubMed: 10553121]

de la Iglesia HO, Meyer J, Schwartz WJ. Lateralization of circadian pacemaker output: Activation of left- and right-sided luteinizing hormone-releasing hormone neurons involves a neural rather than a humoral pathway. The Journal of neuroscience: the official journal of the Society for Neuroscience. 2003; 23(19):7412–7414. [PubMed: 12917377]

de la Iglesia HO, Schwartz WJ. Minireview: timely ovulation: circadian regulation of the female hypothalamo-pituitary-gonadal axis. Endocrinology. 2006; 147(3):1148–1153. [PubMed: 16373412]

Deurveilher S, Burns J, Semba K. Indirect projections from the suprachiasmatic nucleus to the ventrolateral preoptic nucleus: a dual tract-tracing study in rat. The European journal of neuroscience. 2002; 16(7):1195–1213. [PubMed: 12405980]

Deurveilher S, Semba K. Indirect projections from the suprachiasmatic nucleus to the median preoptic nucleus in rat. Brain research. 2003; 987(1):100–106. [PubMed: 14499951]

Deurveilher S, Semba K. Indirect projections from the suprachiasmatic nucleus to major arousal-promoting cell groups in rat: implications for the circadian control of behavioural state. Neuroscience. 2005; 130(1):165–183. [PubMed: 15561433]

Elias CF, Saper CB, Maratos-Flier E, Tritos NA, Lee C, Kelly J, Tatro JB, Hoffman GE, Ollmann MM, Barsh GS, Sakurai T, Yanagisawa M, Elmquist JK. Chemically defined projections linking the mediobasal hypothalamus and the lateral hypothalamic area. The Journal of comparative neurology. 1998; 402(4):442–459. [PubMed: 9862320]

Elmquist JK, Ahima RS, Elias CF, Flier JS, Saper CB. Leptin activates distinct projections from the dorsomedial and ventromedial hypothalamic nuclei. Proceedings of the National Academy of Sciences of the United States of America. 1998; 95(2):741–746. [PubMed: 9435263]

Fuller PM, Lu J, Saper CB. Differential rescue of light- and food-entrainable circadian rhythms. Science (New York, NY). 2008; 320(5879):1074–1077.

Gooley JJ, Lu J, Fischer D, Saper CB. A broad role for melanopsin in nonvisual photoreception. The Journal of neuroscience: the official journal of the Society for Neuroscience. 2003; 23(18):7093–7106. [PubMed: 12904470]

Gooley, JJ.; Saper, CB. Anatomy of the mammalian circadian system. In: Dement, Kryger R., editor. Principles and Practice of Sleep Medicine. 2005. p. 351-362.

Harrington ME. The ventral lateral geniculate nucleus and the intergeniculate leaflet: interrelated structures in the visual and circadian systems. Neuroscience and biobehavioral reviews. 1997; 21(5):705–727. [PubMed: 9353800]

Harrington ME, Rusak B. Lesions of the thalamic intergeniculate leaflet alter hamster circadian rhythms. Journal of biological rhythms. 1986; 1(4):309–325. [PubMed: 2979593]

Hattar S, Kumar M, Park A, Tong P, Tung J, Yau KW, Berson DM. Central projections of melanopsin-expressing retinal ganglion cells in the mouse. The Journal of comparative neurology. 2006; 497(3):326–349. [PubMed: 16736474]

Hawke Z, Ivanov TR, Bechtold DA, Dhillon H, Lowell BB, Luckman SM. PACAP neurons in the hypothalamic ventromedial nucleus are targets of central leptin signaling. The Journal of neuroscience: the official journal of the Society for Neuroscience. 2009; 29(47):14828–14835. [PubMed: 19940178]

Horvath TL. Suprachiasmatic efferents avoid phenestrated capillaries but innervate neuroendocrine cells, including those producing dopamine. Endocrinology. 1997; 138(3):1312–1320. [PubMed: 9048641]

Inouye ST, Kawamura H. Persistence of circadian rhythmicity in a mammalian hypothalamic “island” containing the suprachiasmatic nucleus. Proceedings of the National Academy of Sciences of the United States of America. 1979; 76(11):5962–5966. [PubMed: 293695]

Johnson RF, Morin LP, Moore RY. Retinohypothalamic projections in the hamster and rat demonstrated using cholera toxin. Brain research. 1988; 462(2):301–312. [PubMed: 3191391]

Kalsbeek A, Teclemariam-Mesbah R, Pevet P. Efferent projections of the suprachiasmatic nucleus in the golden hamster (Mesocricetus auratus). The Journal of comparative neurology. 1993; 332(3): 293–314. [PubMed: 8331217]

Kong D, Tong Q, Ye C, Koda S, Fuller PM, Krashes MJ, Vong L, Ray RS, Olson DP, Lowell BB. GABAergic RIP-Cre neurons in the arcuate nucleus selectively regulate energy expenditure. Cell. 2012; 151(3):645–657. [PubMed: 23101631]

Krashes MJ, Koda S, Ye C, Rogan SC, Adams AC, Cusher DS, Maratos-Flier E, Roth BL, Lowell BB. Rapid, reversible activation of AgRP neurons drives feeding behavior in mice. The Journal of clinical investigation. 2011; 121(4):1424–1428. [PubMed: 21364278]

Kriegsfeld LJ, Leak RK, Yackulic CB, LeSauter J, Silver R. Organization of suprachiasmatic nucleus projections in Syrian hamsters (Mesocricetus auratus): an anterograde and retrograde analysis. The Journal of comparative neurology. 2004; 468(3):361–379. [PubMed: 14681931]

Kubota A, Inouye ST, Kawamura H. Reversal of multiunit activity within and outside the suprachiasmatic nucleus in the rat. Neuroscience letters. 1981; 27(3):303–308. [PubMed: 7329635]

Leak RK, Card JP, Moore RY. Suprachiasmatic pacemaker organization analyzed by viral transynaptic transport. Brain research. 1999; 819(1–2):23–32. [PubMed: 10082857]

Leak RK, Moore RY. Topographic organization of suprachiasmatic nucleus projection neurons. The Journal of comparative neurology. 2001; 433(3):312–334. [PubMed: 11298358]

Lechan RM, Molitch ME, Jackson IM. Distribution of immunoreactive human growth hormone-like material and thyrotropin-releasing hormone in the rat central nervous system: evidence for their coexistence in the same neurons. Endocrinology. 1983; 112(3):877–884. [PubMed: 6401625]

Lein ES, Hawrylycz MJ, Ao N, Ayres M, Bensinger A, Bernard A, Boe AF, Boguski MS, Brockway KS, Byrnes EJ, Chen L, Chen TM, Chin MC, Chong J, Crook BE, Czaplinska A, Dang CN, Datta S, Dee NR, Desaki AL, Desta T, Diep E, Dolbeare TA, Donelan MJ, Dong HW, Dougherty JG, Duncan BJ, Ebbert AJ, Eichele G, Estin LK, Faber C, Facer BA, Fields R, Fischer SR, Fliss TP, Frensley C, Gates SN, Glattfelder KJ, Halverson KR, Hart MR, Hohmann JG, Howell MP, Jeung DP, Johnson RA, Karr PT, Kawal R, Kidney JM, Knapik RH, Kuan CL, Lake JH, Laramee AR, Larsen KD, Lau C, Lemon TA, Liang AJ, Liu Y, Luong LT, Michaels J, Morgan JJ, Morgan RJ, Mortrud MT, Mosqueda NF, Ng LL, Ng R, Orta GJ, Overly CC, Pak TH, Parry SE, Pathak SD, Pearson OC, Puchalski RB, Riley ZL, Rockett HR, Rowland SA, Royall JJ, Ruiz MJ, Sarno NR, Schaffnit K, Shapovalova NV, Sivisay T, Slaughterbeck CR, Smith SC, Smith KA, Smith BI, Sodt AJ, Stewart NN, Stumpf KR, Sunkin SM, Sutram M, Tam A, Teemer CD, Thaller C, Thompson CL, Varnam LR, Visel A, Whitlock RM, Wohnoutka PE, Wolkey CK, Wong VY, Wood M, Yaylaoglu MB, Young RC, Youngstrom BL, Yuan XF, Zhang B, Zwingman TA, Jones AR. Genome-wide atlas of gene expression in the adult mouse brain. Nature. 2007; 445(7124):168–176. [PubMed: 17151600]

Levine JD, Weiss ML, Rosenwasser AM, Miselis RR. Retinohypothalamic tract in the female albino rat: a study using horseradish peroxidase conjugated to cholera toxin. The Journal of comparative neurology. 1991; 306(2):344–360. [PubMed: 1711060]

Li X, Gilbert J, Davis FC. Disruption of masking by hypothalamic lesions in Syrian hamsters. Journal of comparative physiology A, Neuroethology, sensory, neural, and behavioral physiology. 2005; 191(1):23–30.

Lin D, Boyle MP, Dollar P, Lee H, Lein ES, Perona P, Anderson DJ. Functional identification of an aggression locus in the mouse hypothalamus. Nature. 2011; 470(7333):221–226. [PubMed: 21307935]

Lu J, Zhang YH, Chou TC, Gaus SE, Elmquist JK, Shiromani P, Saper CB. Contrasting effects of ibotenate lesions of the paraventricular nucleus and subparaventricular zone on sleep-wake cycle and temperature regulation. The Journal of neuroscience: the official journal of the Society for Neuroscience. 2001; 21(13):4864–4874. [PubMed: 11425913]

Meister B, Hokfelt T, Vale WW, Sawchenko PE, Swanson L, Goldstein M. Coexistence of tyrosine hydroxylase and growth hormone-releasing factor in a subpopulation of tubero-infundibular neurons of the rat. Neuroendocrinology. 1986; 42(3):237–247. [PubMed: 2869425]

Moga MM, Moore RY. Organization of neural inputs to the suprachiasmatic nucleus in the rat. The Journal of comparative neurology. 1997; 389(3):508–534. [PubMed: 9414010]

Moore KE. Interactions between prolactin and dopaminergic neurons. Biology of reproduction. 1987; 36(1):47–58. [PubMed: 3552068]

Moore RY, Card JP. Intergeniculate leaflet: an anatomically and functionally distinct subdivision of the lateral geniculate complex. The Journal of comparative neurology. 1994; 344(3):403–430. [PubMed: 8063960]

Moore RY, Eichler VB. Loss of a circadian adrenal corticosterone rhythm following suprachiasmatic lesions in the rat. Brain research. 1972; 42(1):201–206. [PubMed: 5047187]

Moore RY, Speh JC, Leak RK. Suprachiasmatic nucleus organization. Cell and tissue research. 2002; 309(1):89–98. [PubMed: 12111539]

Morin LP, Blanchard JH. Forebrain connections of the hamster intergeniculate leaflet: comparison with those of ventral lateral geniculate nucleus and retina. Visual neuroscience. 1999; 16(6):1037–1054. [PubMed: 10614586]

Morin LP, Goodless-Sanchez N, Smale L, Moore RY. Projections of the suprachiasmatic nuclei, subparaventricular zone and retrochiasmatic area in the golden hamster. Neuroscience. 1994; 61(2):391–410. [PubMed: 7526267]

Nakamura W, Yamazaki S, Nakamura TJ, Shirakawa T, Block GD, Takumi T. In vivo monitoring of circadian timing in freely moving mice. Current biology: CB. 2008; 18(5):381–385. [PubMed: 18334203]

Paxinos, G.; Watson, C. The rat brain in stereotaxic coordinates. Amsterdam; Boston: Elsevier Academic Press; 2005.

Ralph MR, Foster RG, Davis FC, Menaker M. Transplanted suprachiasmatic nucleus determines circadian period. Science (New York, NY). 1990; 247(4945):975–978.

Redlin U, Mrosovsky N. Masking by light in hamsters with SCN lesions. Journal of comparative physiology A, Sensory, neural, and behavioral physiology. 1999; 184(4):439–448.

Saper CB, Fuller PM, Pedersen NP, Lu J, Scammell TE. Sleep state switching. Neuron. 2010; 68(6): 1023–1042. [PubMed: 21172606]

Sato T, Kawamura H. Circadian rhythms in multiple unit activity inside and outside the suprachiasmatic nucleus in the diurnal chipmunk (Eutamias sibiricus). Neuroscience research. 1984; 1(1):45–52. [PubMed: 6543592]

Sawchenko PE, Swanson LW. Immunohistochemical identification of neurons in the paraventricular nucleus of the hypothalamus that project to the medulla or to the spinal cord in the rat. The Journal of comparative neurology. 1982; 205(3):260–272. [PubMed: 6122696]

Schwartz MD, Nunez AA, Smale L. Differences in the suprachiasmatic nucleus and lower subparaventricular zone of diurnal and nocturnal rodents. Neuroscience. 2004; 127(1):13–23. [PubMed: 15219664]

Schwartz MD, Nunez AA, Smale L. Rhythmic cFos expression in the ventral subparaventricular zone influences general activity rhythms in the Nile grass rat, Arvicanthis niloticus. Chronobiology international. 2009; 26(7):1290–1306. [PubMed: 19916832]

Schwartz MD, Urbanski HF, Nunez AA, Smale L. Projections of the suprachiasmatic nucleus and ventral subparaventricular zone in the Nile grass rat (Arvicanthis niloticus). Brain research. 2011; 1367:146–161. [PubMed: 20971082]

Smale L, Castleberry C, Nunez AA. Fos rhythms in the hypothalamus of Rattus and Arvicanthis that exhibit nocturnal and diurnal patterns of rhythmicity. Brain research. 2001; 899(1–2):101–105. [PubMed: 11311870]

Smarr BL, Morris E, de la Iglesia HO. The dorsomedial suprachiasmatic nucleus times circadian expression of Kiss1 and the luteinizing hormone surge. Endocrinology. 2012; 153(6):2839–2850. [PubMed: 22454148]

Standaert DG, Needleman P, Saper CB. Organization of atriopeptin-like immunoreactive neurons in the central nervous system of the rat. The Journal of comparative neurology. 1986; 253(3):315–341. [PubMed: 2947936]

Thompson RH, Swanson LW. Organization of inputs to the dorsomedial nucleus of the hypothalamus: a reexamination with Fluorogold and PHAL in the rat. Brain research Brain research reviews. 1998; 27(2):89–118. [PubMed: 9622601]

Todd WD, Gall AJ, Weiner JA, Blumberg MS. Distinct retinohypothalamic innervation patterns predict the developmental emergence of species-typical circadian phase preference in nocturnal Norway rats and diurnal nile grass rats. The Journal of comparative neurology. 2012; 520(14): 3277–3292. [PubMed: 22431036]

Tong Q, Ye C, McCrimmon RJ, Dhillon H, Choi B, Kramer MD, Yu J, Yang Z, Christiansen LM, Lee CE, Choi CS, Zigman JM, Shulman GI, Sherwin RS, Elmquist JK, Lowell BB. Synaptic glutamate release by ventromedial hypothalamic neurons is part of the neurocircuitry that prevents hypoglycemia. Cell metabolism. 2007; 5(5):383–393. [PubMed: 17488640]

Ueta Y, Fujihara H, Dayanithi G, Kawata M, Murphy D. Specific expression of optically active reporter gene in arginine vasopressin-secreting neurosecretory cells in the hypothalamic-neurohypophyseal system. Journal of neuroendocrinology. 2008; 20(6):660–664. [PubMed: 18601686]

Watts, AG. The Efferent Projections of the Suprachiasmatic Nucleus: Anatomical Insights into the Control of Circadian Rhythms. In: Klein, DC.; Moore, RY.; Reppert, SM., editors. Suprachiasmatic Nucleus: The Mind's Clock. Oxford University Press; 1991.

Watts AG, Sheward WJ, Whale D, Fink G. The effects of knife cuts in the sub-paraventricular zone of the female rat hypothalamus on oestrogen-induced diurnal surges of plasma prolactin and LH, and circadian wheel-running activity. The Journal of endocrinology. 1989; 122(2):593–604. [PubMed: 2769171]

Watts AG, Swanson LW. Efferent projections of the suprachiasmatic nucleus: II. Studies using retrograde transport of fluorescent dyes and simultaneous peptide immunohistochemistry in the rat. The Journal of comparative neurology. 1987; 258(2):230–252. [PubMed: 2438309]

Watts AG, Swanson LW, Sanchez-Watts G. Efferent projections of the suprachiasmatic nucleus: I. Studies using anterograde transport of Phaseolus vulgaris leucoagglutinin in the rat. The Journal of comparative neurology. 1987; 258(2):204–229. [PubMed: 3294923]

Xu Y, Hill JW, Fukuda M, Gautron L, Sohn JW, Kim KW, Lee CE, Choi MJ, Lauzon DA, Dhillon H, Lowell BB, Zigman JM, Zhao JJ, Elmquist JK. PI3K signaling in the ventromedial hypothalamic nucleus is required for normal energy homeostasis. Cell metabolism. 2010; 12(1):88–95. [PubMed: 20620998]

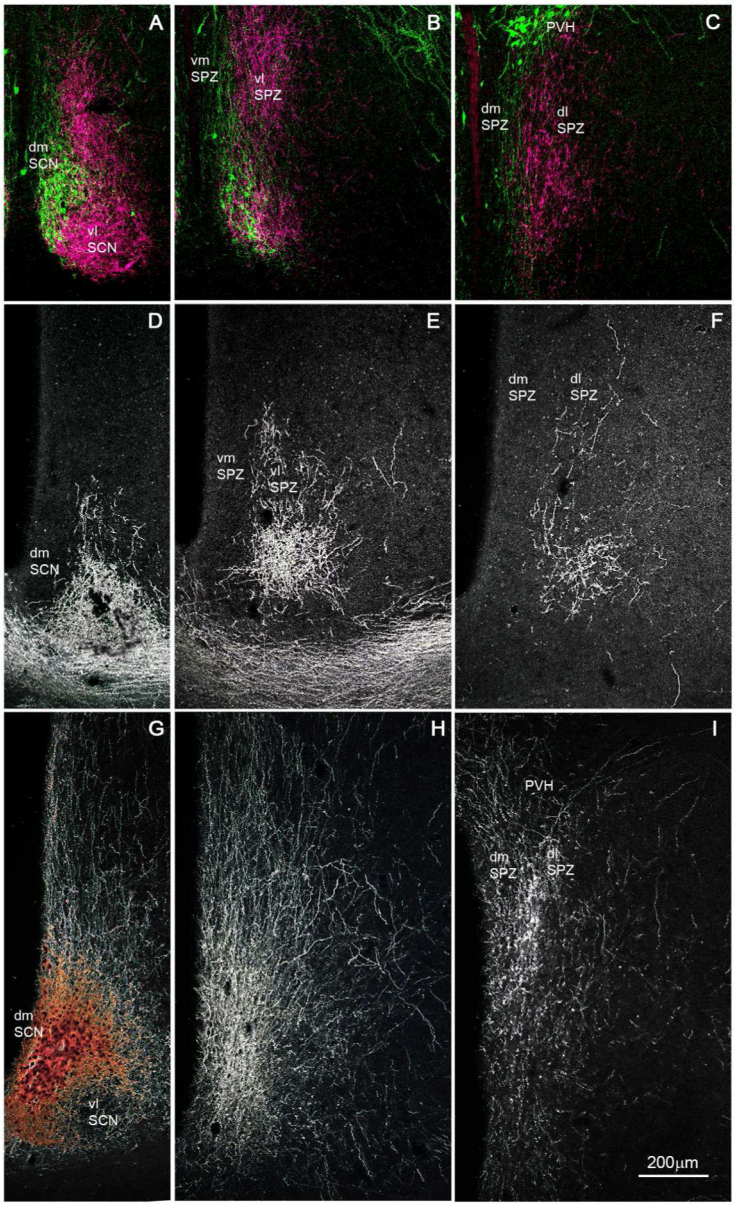

Figure 1.

A series of photomicrographs to illustrate topographic specificity of afferent inputs to the subparaventricular zone. In each row, the photograph at the left (A, D, G) is from the level of the SCN, the one in the middle (B, E, H) is from the level of the rostral/ventral SPZ, and the one on the right (C, F, I) is from the level of the caudal/dorsal SPZ. The first row across (A, B, C) shows afferent from neurons in the SCN expressing arginine vasopressin (green) vs. vasoactive intestinal polypeptide immunoreactivity (magenta). The second row (D, E, F) shows projections from retinal ganglion cells transduced with AAV-GFP (with immunohistochemical enhancement of GFP signal), and the third row (G, H, I) shows inputs from dmSCN neurons transduced with AAV-GFP (with immunohistochemical enhancement of GFP signal).

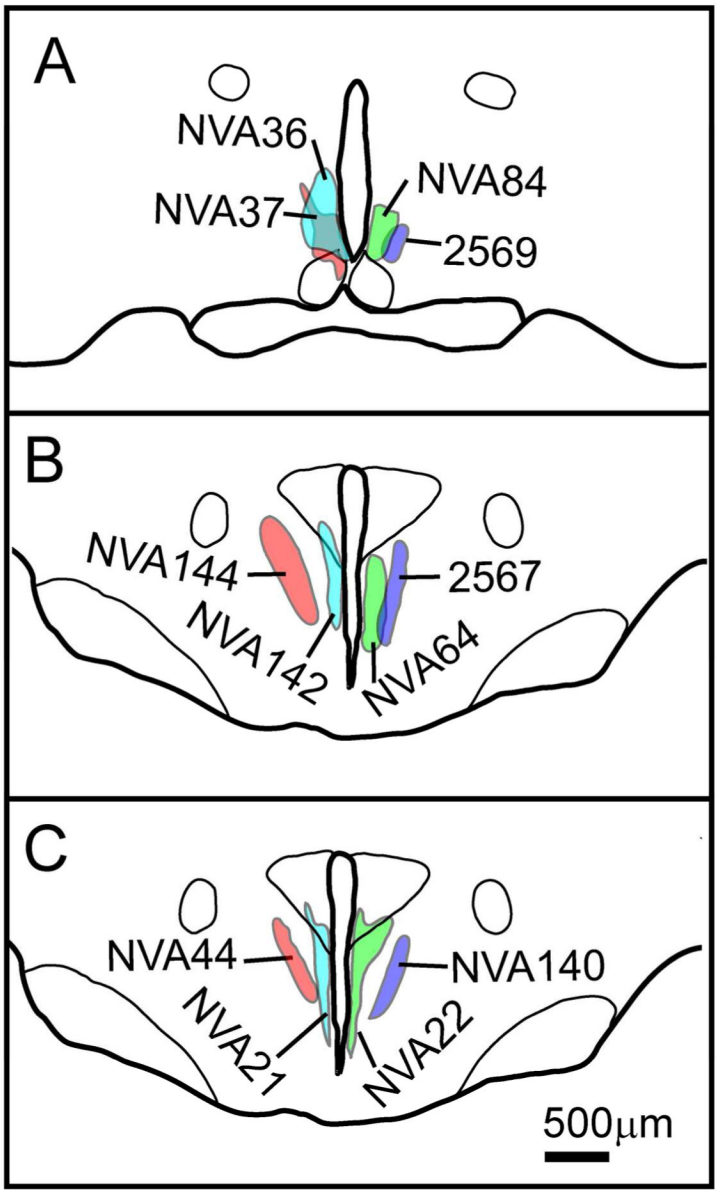

Figure 2.

Camera lucida plots illustrating placement of SPZ injection sites in cases used for comparative analysis across the four SPZ subdivisions at (A) the level of the rostral/ventral SPZ and (B, C) the level of the caudal/dorsal SPZ.

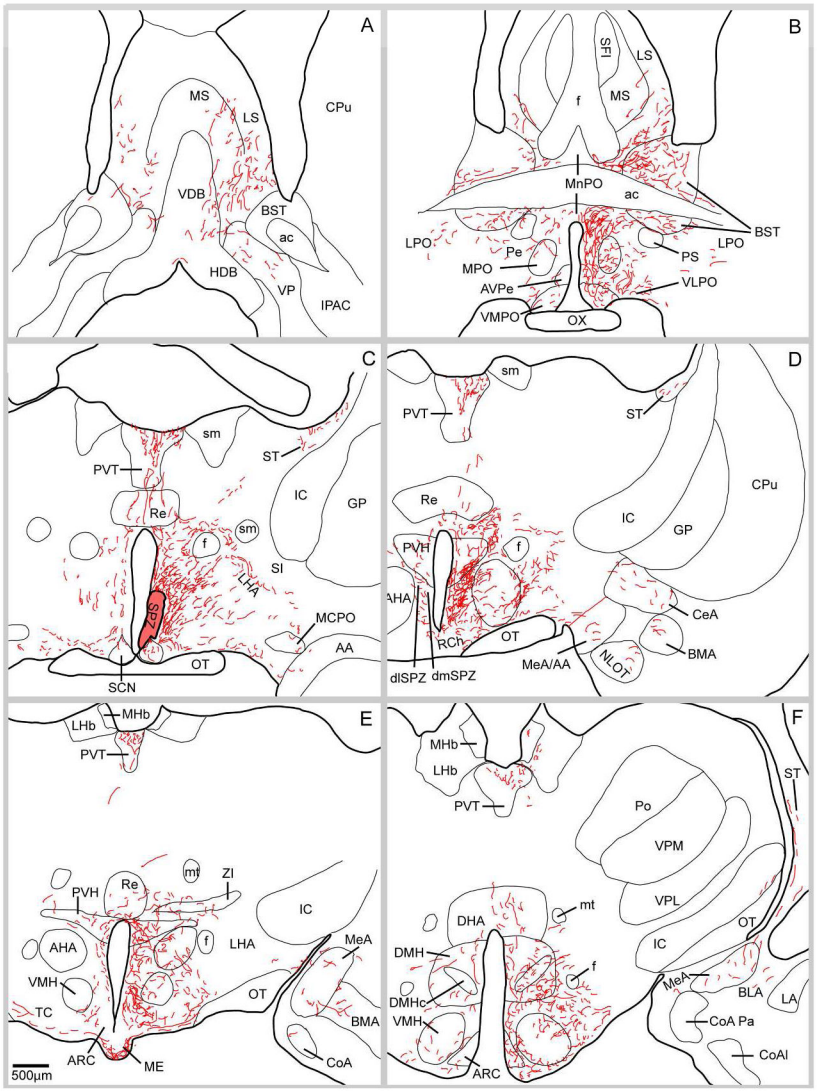

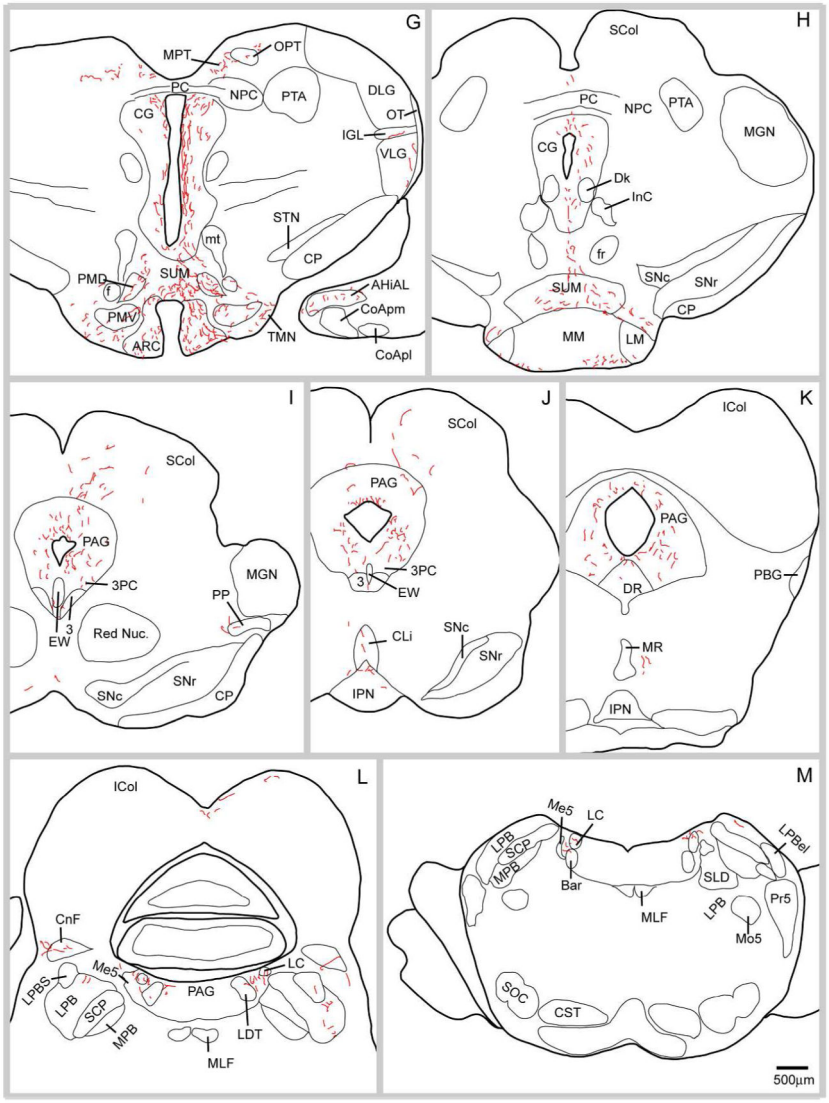

Figure 3.

A series of camera lucida drawings illustrating the pattern of axonal labeling in case NV36. Note the presence of fibers in the dorsal raphe, lateral parabrachial nucleus, pre-coeruleus region, locus coeruleus and Barrington's nucleus.

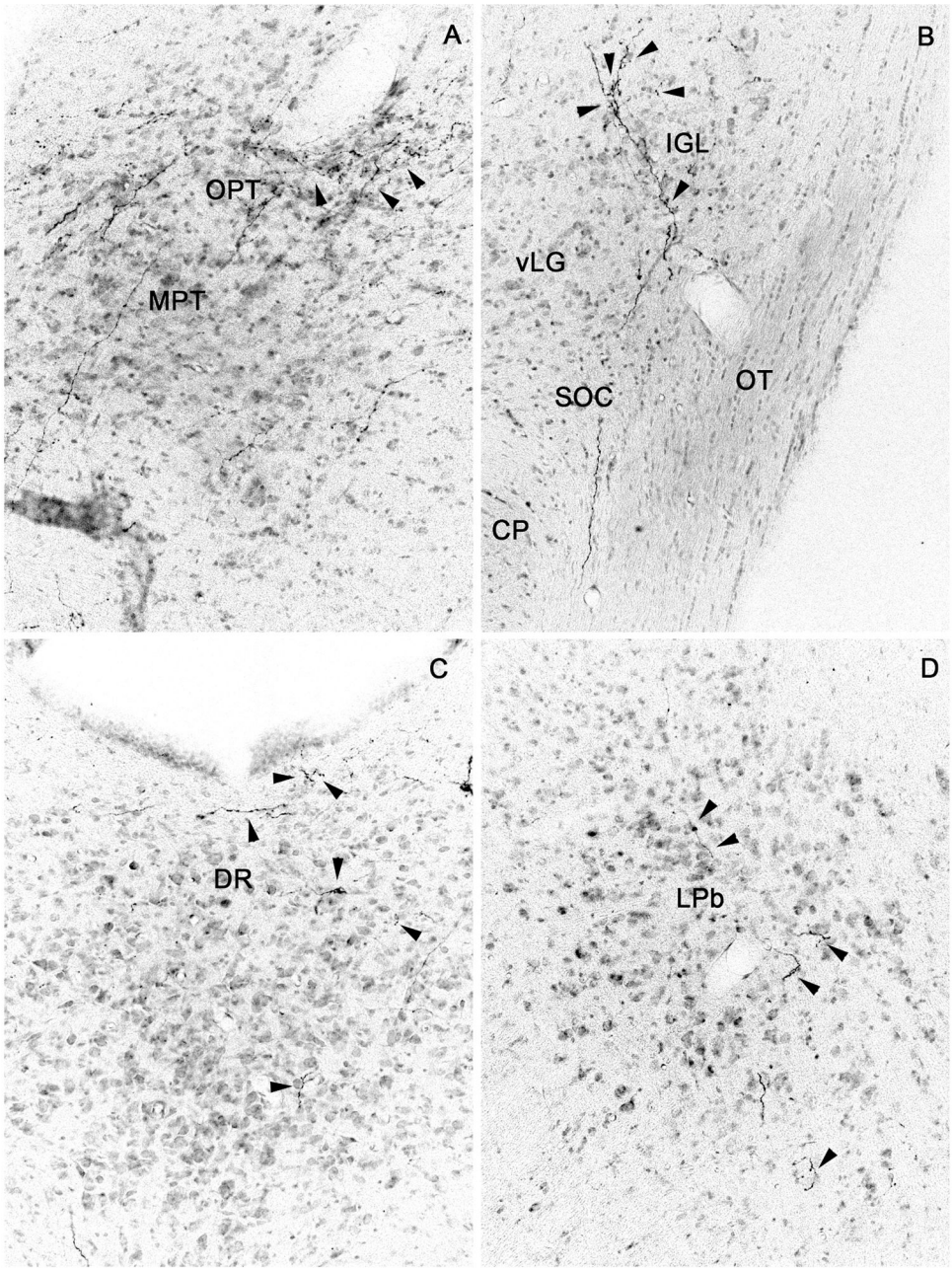

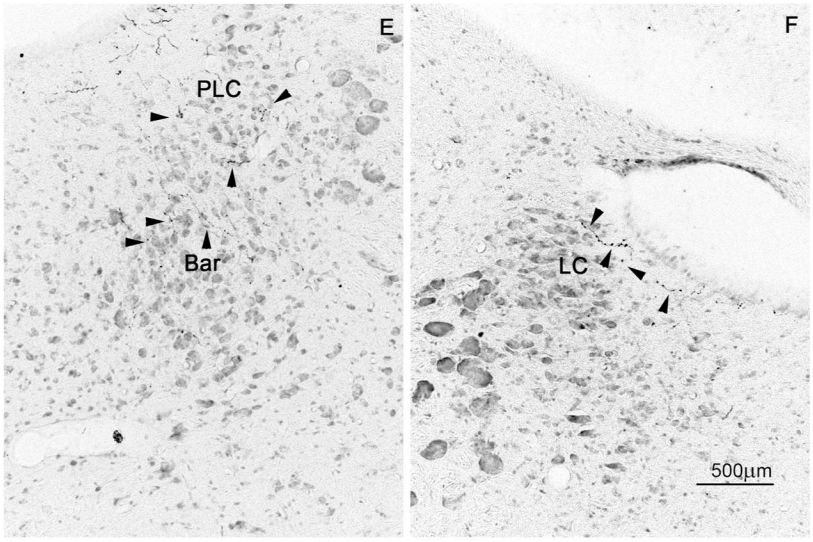

Figure 4.

Brightfield photomicrographs showing distal SPZ projections (from injection case NVA36; cf. drawings in Fig. 3) to (A) the olivary pretectal nucleus, (B) intergeniculate leaflet, (C) dorsal raphe nucleus, (D) lateral parabrachial nucleus, (E) pre-coeruleus area and Barrington's nucleus, and (F) locus coeruleus; black arrowheads indicate axons bearing varicosities or terminal boutons.

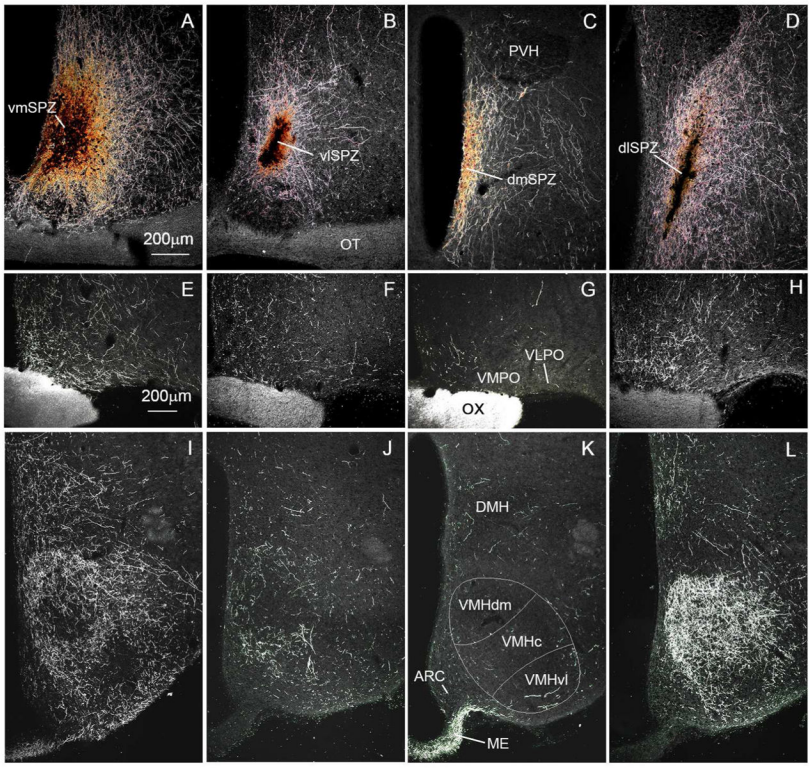

Figure 5.

Darkfield photomicrographs showing (A–D) injection sites (scale bar in A, 200μm) and anterogradely labeled fibers and terminals at the level of the preoptic area (E–H) and ventromedial nucleus of the hypothalamus (I–L; scale bar in E, 200μm). Panels A, E, and I show projections from the vmSPZ (case NVA84); B, F, and J show innervation from the vlSPZ (case 2569); C, G, and K show projections from the dmSPZ (case NVA21); and D, H, and L illustrate output from the dlSPZ (case 2567).

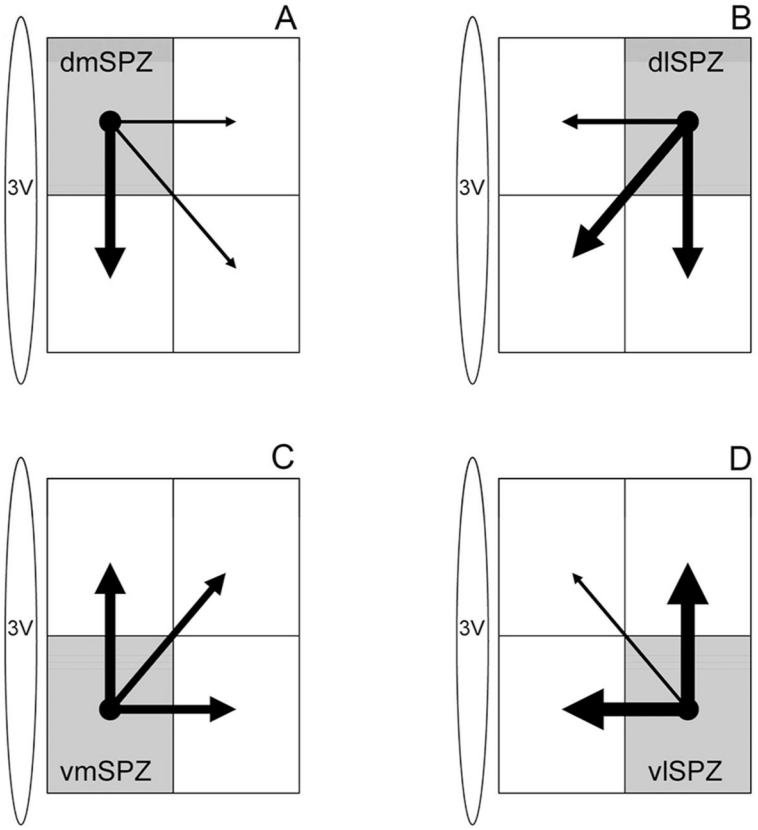

Figure 6.

Schematic diagram illustrating estimated density of intra-SPZ projections based on anterograde tracing from the (A) dorsomedial, (B) dorsolateral, (C) ventromedial, and (D) ventrolateral SPZ. The thickness of each arrow is roughly proportional to the density of the projection.

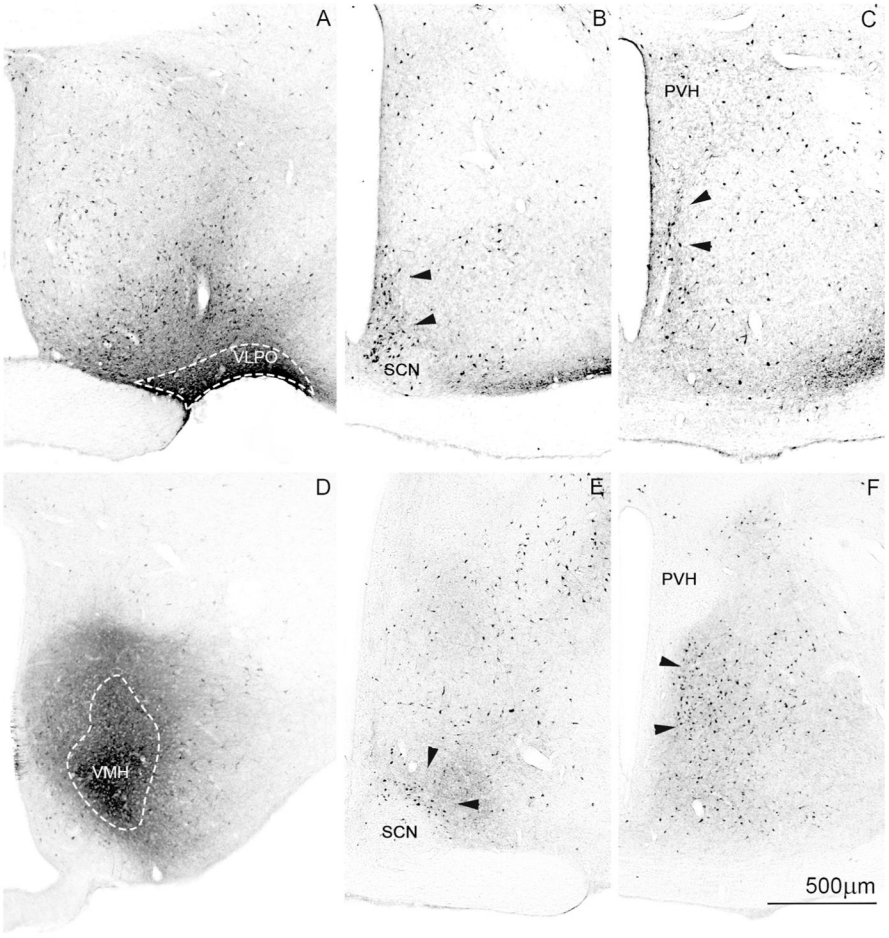

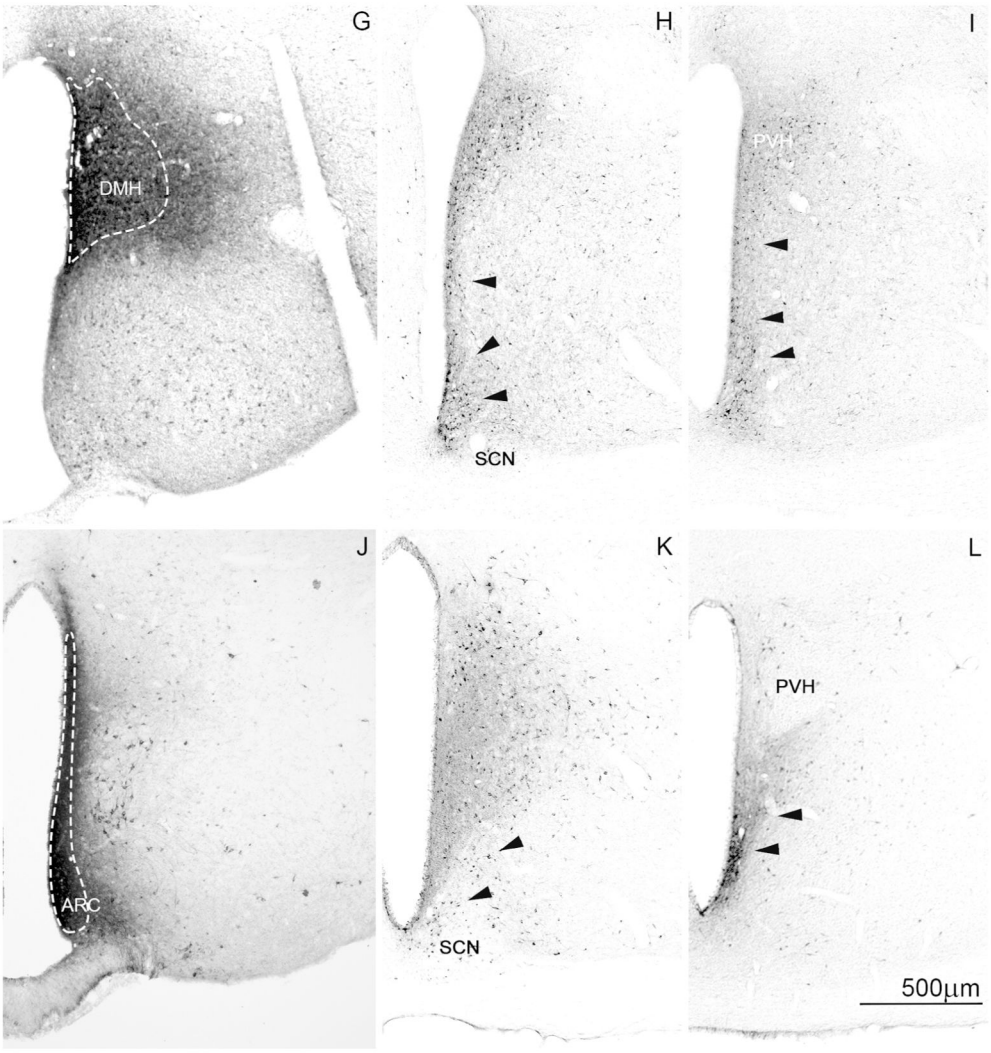

Figure 7.

Brightfield photomicrographs showing injection sites (A,D,G,J) and retrogradely labeled cells at the level of the vSPZ (B,E,H,K) and dSPZ (C,F,H,L) following CTb injection into the (A–C) ventrolateral preoptic nucleus (case R2059), (D–F) ventromedial hypothalamic nucleus (case NVA151), (G–I) dorsomedial hypothalamic nucleus (case 1927), and (J–L) arcuate nucleus (case NVA150). White dotted lines designate the CTb injection core and black arrowheads designate clusters of retrogradely labeled cells in the SPZ.

Table 1

Table of primary antibodies used.

Antigen	Description of Immunogen	Source, Host Species, Cat #, Clone or Lot#, RRID	Concentration used
Cholera Toxin beta subunit (CTb)	CTb protein	Goat, List Biologicals cat#703, RRID:AB_10013220	1:25,000
Green fluorescent protein (GFP)	Aquaphora GFP protein	Rabbit, Molecular probes/Invitrogen ca# A6455, RRID:AB_221570, Lot# 771568	1:20,000
Green fluorescent protein (GFP)	Aquaphora GFP protein	Rabbit, Molecular probes/Invitrogen ca# A11120, RRID:AB_221568, Lot# 71C1-1	1:500
Vasoactive intestinal polypeptide (VIP)	synthetic VIP coupled to bovine thyroglobulin with a carbodiimide linker	Rabbit, ImmunoStar, cat# 20077, RRID:AB_572270, Lot: 722001	1:1,000

Table 2

Projection density from subparaventricular zone subregions

Semiquantitative analysis of density of efferent projections from the four SPZ subregions: dlSPZ description and semiquantitative analysis was based on case 2567, which was compared to NVA140, NVA144, NVA44 for interpretation; vlSPZ description and semiquantitative analysis was based on case 2569; dmSPZ description and semiquantitative analysis was based on case NVA64, which was compared to NVA21, NVA22, NVA142 for interpretation; vmSPZ description and semiquantitative analysis was based on case NVA84, which was compared to NV37 for interpretation.

Region	dlSPZ	vlSPZ	dmSPZ	vmSPZ
Basal Forebrain				
Lateral septal nucleus (LS) (predominantly ventral part)	+++	++	+	+++
Bed nucleus of the stria terminalis (BST)	+++(+)	++(+)	+(+)	+++
Parastrial nucleus (PS)	+++	++	+	+++
Diagonal band of Broca (DBB)	++	++	(+)	+
Organum vasculosum of the lamina terminalis (OVLT)	+	0	(+)	+++
Substantia innominata (SI)	++	0	0	0
Hypothalamus				
Median pre-optic nucleus (MnPO)	(+)	(+)	(+)	+++
Medial pre-optic nucleus (MPO)	++	+	(+)	++
Ventromedial pre-optic nucleus (VMPO)	+++	+	+	++++
Ventrolateral pre-optic nucleus(VLPO)	+ (+)	+(+)	+	++
Suprachiasmatic nucleus (SCN)	+	++(+)	+(+)	+++(+)
Ventromedial subparaventricular zone (vmSPZ)	++	++(+)	+++	n/a
Ventrolateral subparaventricular zone (vlSPZ)	++++	n/a	+	++++
Dorsolateral subparaventricular zone (dlSPZ)	n/a	+++	+(+)	+++
Dorsomedial subparaventricular zone (dmSPZ)	+	+	n/a	+++
Anteroventral periventricular nucleus (AVPe)	+	+	(+)	+++
Anterior hypothalamic area (AHA)	++++	+++	+ (+)	+++
Retrochiasmatic area (RCh)	++(+)	++(+)	+++	++(+)
Supraoptic nucleus (SO)	(+)	+	(+)	+
Supraoptic decussation (Sox)	+++	+(+)	++(+)	+++
Supraoptic nucleus, retrochiasmatic part (SOR)	+++	++	++(+)	+++
Paraventricular nucleus of the hypothalamus (PVH) - anterior parvicellular	+++	++	++(+)	+++(+)
Paraventricular nucleus of the hypothalamus (PVH) - middle	+	+	++	++(+)
Paraventricular nucleus of the hypothalamus (PVH) - lateral wing	++	++	++(+)	+++
Dorsomedial nucleus of the hypothalamus (DMH) - anterior	+++(+)	+++	+(+)	++++
Dorsomedial nucleus of the hypothalamus (DMH) - compact and surrounding	++(+)	++	+(+)	++(+)
Dorsomedial nucleus of the hypothalamus (DMH) - posterior	++	++	+(+)	+(+)
Lateral hypothalamic area (LHA)	+(+)	+	++	++(+)
Ventromedial nucleus of the hypothalamus (VMH) – dorsomedial	+++++	+	+	+++
Ventromedial nucleus of the hypothalamus (VMH) - central	+++++	++	(+)	+(+)
Ventromedial nucleus of the hypothalamus (VMH) - ventrolateral	++++	+++	(+)	+(+)

Region	dlSPZ	vlSPZ	dmSPZ	vmSPZ
Arcuate nucleus of the hypothalamus – medial	+	(+)	+	++(+)
Arcuate nucleus of the hypothalamus – lateral	+++	++	+(+)	+++(+)
Median eminence (ME)	+	+	++++	+++
Supramammillary nucleus (SUM)	+++	+	(+)	++
Medial mammillary nucleus (MM)	++	+	(+)	(+)
Mammillary body (edges)	++	++	++	+++
Tuberomammillary nucleus (TMN)	++(+)	++	+	++
Posterior hypothalamus	++(+)	+	(+)	++
Pons and brainstem				
Periaqueductal/central gray (PAG/CG)	+++(+)	+++(+)	(+)	+++
Ventral tegmental area (VTA)	++	+	+	+
Substantia nigra (SN)	(+)	(+)	(+)	(+)
Dorsal raphe nucleus (DR)	(+)	n/a	0	+
Pre-coeruleus	(+)	n/a	(+)	+
Locus coeruleus (LC)	0	n/a	0	(+)
Parabrachial nucleus (PB)	+	n/a	(+)	+(+)
Thalamus and habenula				
Paraventricular nucleus of the thalamus (PVT) - anterior	+++	++(+)	+	++++
Paraventricular nucleus of the thalamus (PVT) - middle	+++	+	(+)	++++
Paraventricular nucleus of the thalamus (PVT) - posterior	++	+	(+)	+++
Habenular nucleus of the nucleus (Hb)	+(+)	+(+)	0	(+)
Paratenial nucleus of the thalamus	++	++	(+)	++
Reuniens nucleus of the thalamus (Re)	+	++	(+)	++(+)
Intergeniculate leaflet (IGL)	(+)	+(+)	0	+
Lateral geniculate nucleus of the thalamus (LGN)	(+)	(+)	0	+(+)
Cortical structures				
Medial nucleus of the Amygdala (MeA)	++	+(+)	++	++
Central nucleus of the Amygdala (CeA)	+	0	+	+